NorthWest Research Associates, Inc.
P.O. Box 3027 • Bellevue, WA 98009-3027

R.L. (2)

NWRA-CR-93-R103

INERTIAL INSTABILITY OF NONPARALLEL FLOW ON AN EQUATORIAL BETA-PLANE

Timothy J. Dunkerton
Northwest Research Associates, Inc.
P.O. Box 3027
Bellevue, WA 98009

14 June 1993

Annual Technical Report for Period 15 May 1992 - 14 May 1993
Contract #F49620-92-C-0033

Prepared for:
AIR FORCE OFFICE OF SCIENTIFIC RESEARCH
Bolling AFB
Washington, DC 20332

REPORT DOCUMENTATION PAGE

Form Approved
OMB No. 0704-0188

1. AGENCY USE ONLY (Leave blank)	2. REPORT DATE	3. REPORT TYPE AND DATES COVERED
	14 JUN 93	Annual Technical Rpt. 15May92-14May93

4. TITLE AND SUBTITLE
Inertial Instability of Nonparallel Flow on an Equatorial Beta-Plane

5. FUNDING NUMBERS
Contract
F49620-92-C-0033
61102F
2310
CB

6. AUTHOR(S)
Timothy J. Dunkerton

7. PERFORMING ORGANIZATION NAME(S) AND ADDRESS(ES)
Northwest Research Associates, Inc.
P.O. Box 3027
Bellevue, WA 98009

8. PERFORMING ORGANIZATION REPORT NUMBER
NWRA-CR-93-R103

9. SPONSORING/MONITORING AGENCY NAME(S) AND ADDRESS(ES)
Air Force Office of Scientific Research
Bolling AFB
Washington, DC 20332
Program Manager: Maj. James Kroll

10. SPONSORING/MONITORING AGENCY REPORT NUMBER

11. SUPPLEMENTARY NOTES

12a. DISTRIBUTION/AVAILABILITY STATEMENT
Approved for public release;
distribution unlimited.

12b. DISTRIBUTION CODE

13. ABSTRACT *(Maximum 200 words)*

A simple theoretical model was developed to investigate the inertial instability of zonally nonuniform, nonparallel flow near the equator. The basic state was independent of height and time but included cross-equatorial shear with longitudinal variation, as observed in the tropical mesosphere and elsewhere. Numerical solutions were obtained for the most unstable modes. It is shown that, in addition to previously known 'global' (symmetric and nonsymmetric) modes of inertial instability, there exist 'local' modes within regions of anomalous potential vorticity. The local mode has properties similar to those of 'absolute' instability of nonparallel flow as discussed elsewhere in fluid dynamics.

14. SUBJECT TERMS	15. NUMBER OF PAGES
inertial instability, equatorial inertia-gravity waves	54
	16. PRICE CODE

17. SECURITY CLASSIFICATION OF REPORT	18. SECURITY CLASSIFICATION OF THIS PAGE	19. SECURITY CLASSIFICATION OF ABSTRACT	20. LIMITATION OF ABSTRACT
Unclassified	Unclassified	Unclassified	

NSN 7540-01-280-5500

Standard Form 298 (Rev. 2-89)
Prescribed by ANSI Std. Z39-18
298-102

Summary

The research supported under Contract F49620-92-C-0033 represents an effort to understand, through observational, numerical, and theoretical means, the role of unbalanced motions such as gravity waves, inertia-gravity waves, equatorially trapped waves and inertial instabilities in the earth's atmosphere, and to develop suitable parameterizations of their effects. These waves and instabilities redistribute momentum vertically and/or horizontally and irreversibly alter the distribution of momentum, heat and trace constituents when undergoing turbulent breakdown and absorption.

This report continues our investigation with a theoretical study of equatorial inertial instability. In addition to the material presented herein, we are currently engaged in studies of gravity and equatorial wave excitation by latent heating in the tropical atmosphere, and the role of gravity wave drag in the bifurcation properties of the polar vortex in the winter middle atmosphere. These areas are being investigated in collaboration with Drs. Francis Crum and Donal O'Sullivan of NWRA, who have been partially supported by the AFOSR Contract. The substance of these investigations will be reported later.

TABLE OF CONTENTS

LIST OF FIGURES

1. Introduction

Inertial instability may arise in conservative axisymmetric flow near the equator when there is nonzero latitudinal shear $\gamma = \bar{u}_y$. In this case potential vorticity (PV) on one side of the equator is anomalous, satisfying a necessary condition for centrifugal parcel instability (Dunkerton, 1981). Analytic eigenmodes of symmetric instability in zonally uniform shear on an equatorial beta-plane were obtained by Dunkerton and independently by Stevens (1983). Subsequently Boyd and Christidis (1982) and Dunkerton (1983) found that low-wavenumber, zonally nonsymmetric instabilities have larger growth rates than symmetric instability when (a) the vertical wavenumber m is near or below a neutral point of symmetric instability

$$\frac{|m|}{N} = \epsilon_{\text{neut}}^{1/2} = \frac{4\beta}{\gamma^2} \tag{1.1}$$

(N is static stability and $\beta = 2\Omega/a = 2.29{\cdot}10^{-11}\text{m}^{-1}\text{s}^{-1}$) and (b) there exist nonzero *integer* zonal wavenumbers $s = ka$ below a short-wave cutoff $k_{\text{max}} \equiv \beta/\gamma$. Although symmetric instability has maximum inviscid growth approaching $\gamma/2$ as $|m| \to \infty$, the nonsymmetric mode is preferred when second-order viscosity and diffusion are added and conditions (a,b) are met (Dunkerton, 1983). Similar conclusions pertain to midlatitude flow containing nonsymmetric inertial and barotropic instabilities as shown by Stevens and Ciesielski (1986).

Anomalous PV exists in the tropical winter mesosphere (Dunkerton, 1981; Hitchman and Leovy, 1986), upper troposphere between South America and Indian Ocean (Liebmann, 1987), lower troposphere near Indonesia (Krishnamurti *et al*, 1985, 1988), and Pacific south equatorial current (Philander, 1989, p. 62). Inertial instabilities were found in a nearly inviscid 2D axisymmetric model of the troposphere (Held and Hou, 1980) and in 3D middle atmosphere GCMs (Hunt, 1981; O'Sullivan and Hitchman, 1992). This instability was suggested as a possible explanation of layered structures in the tropical mesosphere (Hitchman *et al*, 1987; Fritts *et al*, 1992) and mesoscale anomalies in the midlatitude upper troposphere (Ciesielski *et al*, 1989). Conditional 'symmetric' instability is thought to explain frontal rainbands according to Bennetts and Hoskins (1979) and several others.

Unfortunately for the theory, none of the regions of anomalous PV in atmosphere or ocean are zonally symmetric. Observations and numerical models suggest, for example, that inertial instabilities in the mesosphere coincide with tropical penetration of planetary Rossby waves from midlatitudes (Hitchman *et al*, 1987; O'Sullivan and Hitchman, 1992). For the theory to be relevant, it must be generalized to a nonparallel or zonally nonuniform basic state.

The purpose of this paper is to develop a simple theoretical formalism and thereby to document two types of inertial instability in nonparallel flow: 'local' instability (stationary and zonally propagating) and 'global' instability (symmetric and nonsymmetric). Of these, the local instabilities are new and probably most relevant to middle atmosphere models in which breaking planetary waves produce regions of significantly anomalous PV near the equator.

The theoretical model is described in Section 2 including a brief review of symmetric and nonsymmetric instability. Growth rates and structure of nonparallel instabilities are illustrated in Section 3 for a wide range of model parameters using a simple analytic basic state resembling the onset of planetary wavebreaking. The theoretical interpretation of local instability is discussed further in Section 4 and the Appendix.

2. Background

To isolate the effect of horizontal basic state variations, a simple two-dimensional (x-y) model is desirable, analogous to the shallow-water system. In a vertically continuous atmosphere, these equations describe perturbations oscillating in height with constant sinusoidal variation. Vertical wavelength is then contained in Lamb's parameter ϵ (Andrews *et al*, 1987) and is specified *a priori*. In this section, the simple model is developed, its solution method described, and a brief review given of parallel flow instabilities (several features of which carry over to the nonparallel case).

a. Theoretical model

The hydrostatic primitive equations on an equatorial beta-plane are

$$u_t + uu_x + v(u_y - \beta y) + wu_z + \phi_x = X \tag{2.1a}$$

$$v_t + u(v_x + \beta y) + vv_y + wv_z + \phi_y = Y \tag{2.1b}$$

$$\phi_{zt} + u\phi_{xz} + v\phi_{zy} + w(N^2 + \phi_{zz}) = Q \tag{2.1c}$$

$$u_x + v_y + \frac{1}{\rho_0}(\rho_0 w)_z = 0 \tag{2.1d}$$

where u,v,w are zonal, meridional, and vertical velocity, ϕ is geopotential, ρ_0 is basic state density $\rho_s \exp(-z/H)$, and X, Y, Q are dissipative terms. Eqs. (2.1) are essentially those of Andrews and McIntyre (1976) written in log-pressure notation of Holton (1975).

To formulate an idealized model of instability the dependent variables may be expanded as

$$u(x,y,z,t) = \tilde{U}(x,y) + u'(x,y,z,t) \tag{2.2}$$

and similarly for v,w,ϕ. $\tilde{U}(x,y)$ is a barotropic basic state independent of height and time for the purpose of linear stability analysis. Linearized perturbation equations are then

$$u'_t + \bar{u}u'_x + v'(\bar{u}_y - \beta y) + \phi'_x = A + K\nabla_H^2 u' - \nu m^2 u' \tag{2.3a}$$

$$v'_t + \bar{u}v'_x + \beta y u' + \phi'_y = B + K\nabla_H^2 v' - \nu m^2 v' \tag{2.3b}$$

$$\phi'_t + \bar{u}\phi'_x + \epsilon^{-1}(u'_x + v'_y) = C + K\nabla_H^2 \phi' - \nu m^2 \phi' \tag{2.3c}$$

under the following assumptions:

1) The basic state velocity field is barotropic, temporally constant, and horizontal ($\tilde{W} \equiv 0$). More generally we could regard the mean flow as slowly varying in height and time (Boyd, 1978).

2) Advection of basic-state temperature is neglected, i.e. $\mathbf{u}' \cdot \nabla_H \Phi_z = 0$. This term has a counterpart $\mathbf{u}' \cdot \nabla_H \Phi$ normally retained in the shallow-water system.[1]

3) Perturbations vary as $\exp imz$, and $m^2 \gg 1/(4H^2)$ whereupon $\epsilon \approx m^2/N^2$ as in (1.1).

4) $|\phi_{zz}| \ll N^2$.

5) Dissipative terms are written as second-order viscosity and diffusion.

In (2.3a-c) the zonally symmetric component of $\tilde{U}$ was kept on the lhs, i.e.

$$\tilde{U} \to \bar{u}(y) + U(x,y) \tag{2.4a}$$

$$\tilde{V} \to \qquad V(x,y) \tag{2.4b}$$

and on the rhs

$$-A \equiv (Uu'_x + Vu'_y) + (u'U_x + v'U_y) \tag{2.5a}$$

$$-B \equiv (Uv'_x + Vv'_y) + (u'V_x + v'V_y) \tag{2.5b}$$

$$-C \equiv (U\phi'_x + V\phi'_y) \tag{2.5c}$$

b. Solution method

To solve (2.3a-c) a semi-implicit method was used in which variables were expanded in zonal harmonics (letting k be integers for the moment)

[1] In real atmospheres the basic state will include variations of static stability induced by potential vorticity anomalies (Hoskins *et al*, 1985). For simplicity, only the variation of induced horizontal velocity U, V was retained in the definition of A, B, C. This assumption is reasonable in the tropical middle atmosphere where incident Rossby waves have approximately horizontal ray paths.

$$\begin{Bmatrix} u' \\ v' \\ \phi' \end{Bmatrix} \equiv \frac{1}{2}\sum_{k=-\infty}^{\infty} \begin{Bmatrix} u_k \\ iv_k \\ \phi_k \end{Bmatrix} \exp\frac{ikx}{a} \tag{2.6a}$$

$$\begin{Bmatrix} U \\ V \end{Bmatrix} \equiv \frac{1}{2}\sum_{k\neq 0} \begin{Bmatrix} U_k \\ V_k \end{Bmatrix} \exp\frac{ikx}{a} \tag{2.6b}$$

$$\begin{Bmatrix} A \\ B \\ C \end{Bmatrix} \equiv \frac{1}{2}\sum_{k=-\infty}^{\infty} \begin{Bmatrix} A_k \\ B_k \\ C_k \end{Bmatrix} \exp\frac{ikx}{a} \tag{2.6c}$$

Terms on the lhs of (2.3a-c) were treated implicitly in time, i.e.

$$\hat{u}_k = \frac{1}{2}(u_k^n + u_k^{n+1}), \text{etc.} \tag{2.7}$$

so that for each harmonic

$$-\hat{\omega}\hat{u}_k + \hat{v}_k(\bar{u}_y - \beta y) + \frac{k}{a}\hat{\phi}_k = -i\tilde{A}_k^n - \omega u_k^n \tag{2.8a}$$

$$+\hat{\omega}\hat{v}_k + \beta y\hat{u}_k + \frac{\partial}{\partial y}\hat{\phi}_k = \tilde{B}_k^n + \omega v_k^n \tag{2.8b}$$

$$-\hat{\omega}\hat{\phi}_k + \epsilon^{-1}\left(\frac{k}{a}\hat{u}_k + \frac{\partial}{\partial y}\hat{v}_k\right) = -i\tilde{C}_k^n - \omega\phi_k^n \tag{2.8c}$$

where $\hat{\omega} \equiv \omega - k\bar{u}/a$, $\omega \equiv 2i/\Delta t$, and

$$\tilde{A}_k = A_k + \text{diffusion terms, etc.} \tag{2.9}$$

After some manipulation (2.8a-c) reduce to a geopotential equation

$$\Delta\frac{\partial}{\partial y}\left(\frac{\phi_y}{\Delta}\right) - \phi\left[k^2 + \frac{k\beta}{\hat{\omega}\Delta}(y\Delta_y - \Delta)\right] = \epsilon\Delta\phi + D \tag{2.10}$$

for each harmonic, where

$$\Delta \equiv \beta y(\beta y - \gamma) - \hat{\omega}^2. \tag{2.11}$$

D, whose definition is omitted for brevity, includes the explicit forcing and solutions from previous time step. Eq. (2.10) was solved by discretizing in y with 64 grid points and using a tridiagonal algorithm. The domain was periodic in x and extended from $-4y_s$ to $+6y_s$ where $y_s \equiv \gamma/2\beta$. There are no critical latitude ($\hat{\omega} = 0$) or inertial latitude ($\Delta = 0$) singularities when $\hat{\omega}$ is complex. A spectral rather than pseudospectral method was used to evaluate D since in this case U_k, $V_k \equiv 0$ for any $|k| \neq 1$, that is, a purely wave 1 contribution to basic state variation in x was assumed. Product terms A_k, etc. could be determined efficiently without transforms. In the numerical integrations

$$\bar{u} = \gamma(y - y_c) + \bar{u}_0 \tag{2.12}$$

where γ and $\bar{u}_0$ are constants. Fields of U, V are specified in Section 3.

c. Instability of uniform parallel flow

When $U = V = 0$, harmonic perturbations $\propto \exp i(kx - \omega t)$ satisfy

$$-\hat{\omega}u + v(\gamma - \beta y) + k\phi = 0 \tag{2.13a}$$

$$+\hat{\omega}v + \beta y u + \phi_y = 0 \tag{2.13b}$$

$$-\hat{\omega}\epsilon\phi + ku + v_y = 0 \tag{2.13c}$$

where $\hat{\omega} = \omega - k\bar{u}$. The geopotential equation derived from (2.13a-c) is just (2.10) with $D \equiv 0$ and $\hat{\omega}$ redefined as intrinsic frequency. This equation is linear in the 'eigenvalue' ϵ. Boyd (1978) derived the meridional velocity equation

$$v_{yy} + \frac{2\epsilon\hat{\omega}k\gamma}{\epsilon\hat{\omega}^2 - k^2}v_y - v\left[\frac{k}{\hat{\omega}}(\beta - \gamma_y) + k^2 + \epsilon\Delta + \frac{2\epsilon k^2\gamma(\beta y - \gamma)}{\epsilon\hat{\omega}^2 - k^2}\right] = 0 \tag{2.14}$$

which is nonlinear in ϵ unless, for example, $\epsilon\hat{\omega}^2 \gg k^2$ in which case

$$v_{yy} + \frac{2k\gamma}{\hat{\omega}}v_y - v\left[\frac{k}{\hat{\omega}}(\beta - \gamma_y) + \epsilon\Delta\right] \approx 0 \tag{2.15}$$

If $k = 0$

$$v_{yy} - \epsilon v\left[\beta y(\beta y - \gamma) - \omega^2\right] = 0 \tag{2.16}$$

and the eigencondition for symmetric instability is

$$\omega^2 + \gamma^2/4 = \frac{(2n+1)N\beta}{|m|} \tag{2.17}$$

(Dunkerton, 1981). Solutions for v are Hermite functions (polynomials times a Gaussian) centered about a 'shifted equator' $y_s \equiv \gamma/2\beta$, the center of anomalous vorticity region. For $n = 0$ the neutral point of symmetric instability (hereafter, 'neutral point') is given by (1.1). For small k and $\gamma_y = 0$,

$$\omega^2 + \gamma^2/4 \approx \frac{N\beta}{|m|} + \frac{k\beta}{\omega\epsilon} \tag{2.18a}$$

At $\epsilon = \epsilon_{neut}$,

$$\omega^3 \approx \frac{k\beta}{\epsilon} \tag{2.18b}$$

Eqs. (2.18a,b) were derived in nondimensional form by Boyd and Christidis (1982).

At finite k the eigenproblem (2.10) or (2.14) must be solved numerically. Growth rates for $\gamma = 10^{-5}\mathrm{s}^{-1}$ are shown in Fig. 1 illustrating the relative importance of symmetric and nonsymmetric modes. Curves were obtained from the geopotential equation by a shooting method; symbols correspond to values from the time-dependent model. They are in excellent agreement except at very small growth rates, where the time-dependent model could not determine growth rate accurately, and at large ϵ, where latitudinal resolution was inadequate.

An approximate model derived from (2.15) contains eigenfrequencies similar to the exact values of Fig. 1 over a large portion of parameter space. This model begins with constant γ and assumes that y-variations of intrinsic frequency can be neglected outside Δ:

$$v_{yy} + \frac{2k\gamma}{\omega_0} v_y - v\left[\frac{k\beta}{\omega_0} + \epsilon\Delta\right] \approx 0 \tag{2.19}$$

where ω_0 is a constant (complex) intrinsic frequency within the unstable region. It follows that

$$\frac{(\omega - k\gamma^2/\beta)^2}{1 - k^2\gamma^2/\beta^2} + \frac{1}{4}\gamma^2 = \frac{N\beta}{|m|}\sqrt{1 - k^2\gamma^2/\beta^2} + \frac{k\beta}{\omega_0\epsilon} \tag{2.20}$$

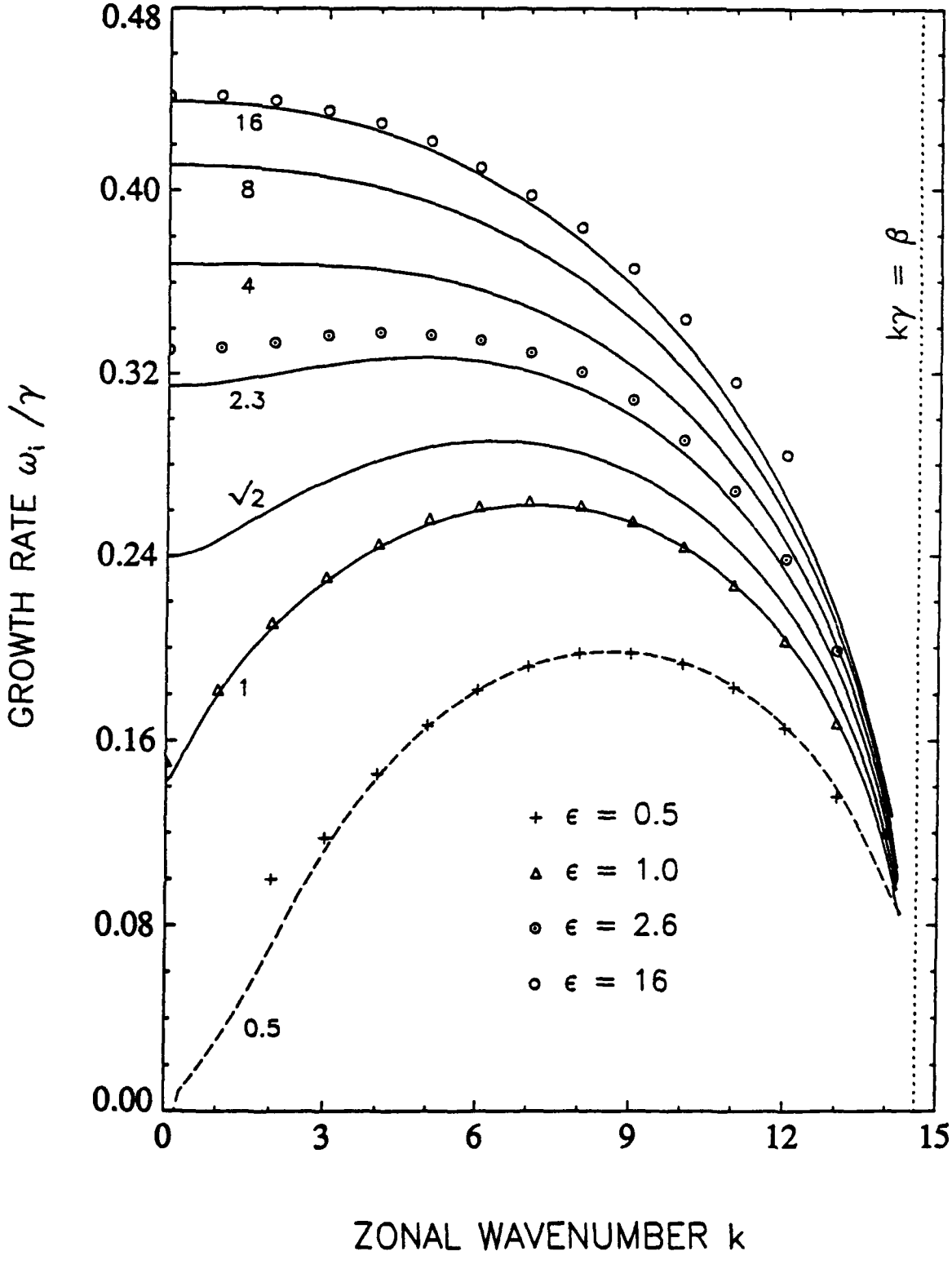

Fig. 1: Growth rate as a function of zonal wavenumber in parallel flow, for $\gamma = 10^{-6} s^{-1}$; ϵ in units $m^{-2}s^2$. Symbols denote results of time-dependent numerical model; solid and dashed curves show analytic results from a shooting method. (The dashed curve had no symmetric instability because $\epsilon < \epsilon_{neut}$.)

where

$$\omega_0 \equiv \omega - k\gamma^2 \frac{\beta - 2\omega k}{2(\beta^2 - k^2\gamma^2)} \tag{2.21}$$

A formal justification of approximations leading to (2.20) will not be given except to note that terms of $O(k^2\gamma^2)$ arise from Δ at large y and cannot be ignored for latitudinal trapping and quantization of eigenfunctions near the short-wave cutoff. The approximate dispersion relation (2.20) has the desired behavior at small and large k. In between, agreement with exact growth rates and phase speeds is good for $\epsilon \geq \epsilon_{\text{neut}}$ (not shown). At smaller ϵ the cubic equation fails in two ways: growth rates are overestimated at intermediate k and there is no Kelvin wave instability at small k below the neutral point (Boyd and Christidis, 1982).

3. Instability of nonparallel flow

The time-dependent model of Section 2 was used to determine the growth of unstable modes in nonparallel flow. Some characteristics of these modes are now described. The basic state, independent of height and time, was designed as a simple analog of incipient planetary wavebreaking in the tropical mesosphere. The evolution of inertial instability in a time-dependent Rossby-wave critical layer was recently discussed by O'Sullivan and Hitchman (1992) in a three-dimensional model. In order to understand the selection of unstable modes it will be worthwhile to explore the parameter dependence of inertial instability in a simpler two-dimensional model.

a. Basic state

The basic state was defined by

$$\bar{u}(y) + U(x,y) = \gamma(y - y_c) - \frac{\gamma\psi y_s}{2}\left[1 + \tanh\left(\frac{y - y_c}{y_s}\right)\right]\cos(x/a) + \bar{u}_0 \qquad (3.1)$$

In (3.1), the latitude of maximum shear is y_c, ψ is dimensionless amplitude of basic state variation, $y_s = \gamma/2\beta$ is the center of anomalous zonal-mean vorticity as defined previously, and $\bar{u}_0$ is a constant mean flow independent of x, y. The profile (3.1) is shown in Fig. 2 for $y_c = 1.8y_s$, $\psi = 1$, and $\bar{u}_0 = 0$.

In Fig. 2, latitudinal shear at $y = y_c$ was increased (decreased) relative to the zonal mean by 50% at 180 (0) degrees longitude. The flow was inertially unstable at all x, but more so at the center of figure. This region could represent a zone of enhanced latitudinal shear set up by Rossby waves penetrating from latitudes north of the equator. In reality there would be some latitudinal phase tilt during critical layer development (O'Sullivan and Hitchman, 1992) – an unnecessary complication for stability analysis.

The meridional component of basic state $V(x,y)$ was included in all simulations, i.e.,

$$U_x + V_y = 0. \qquad (3.2)$$

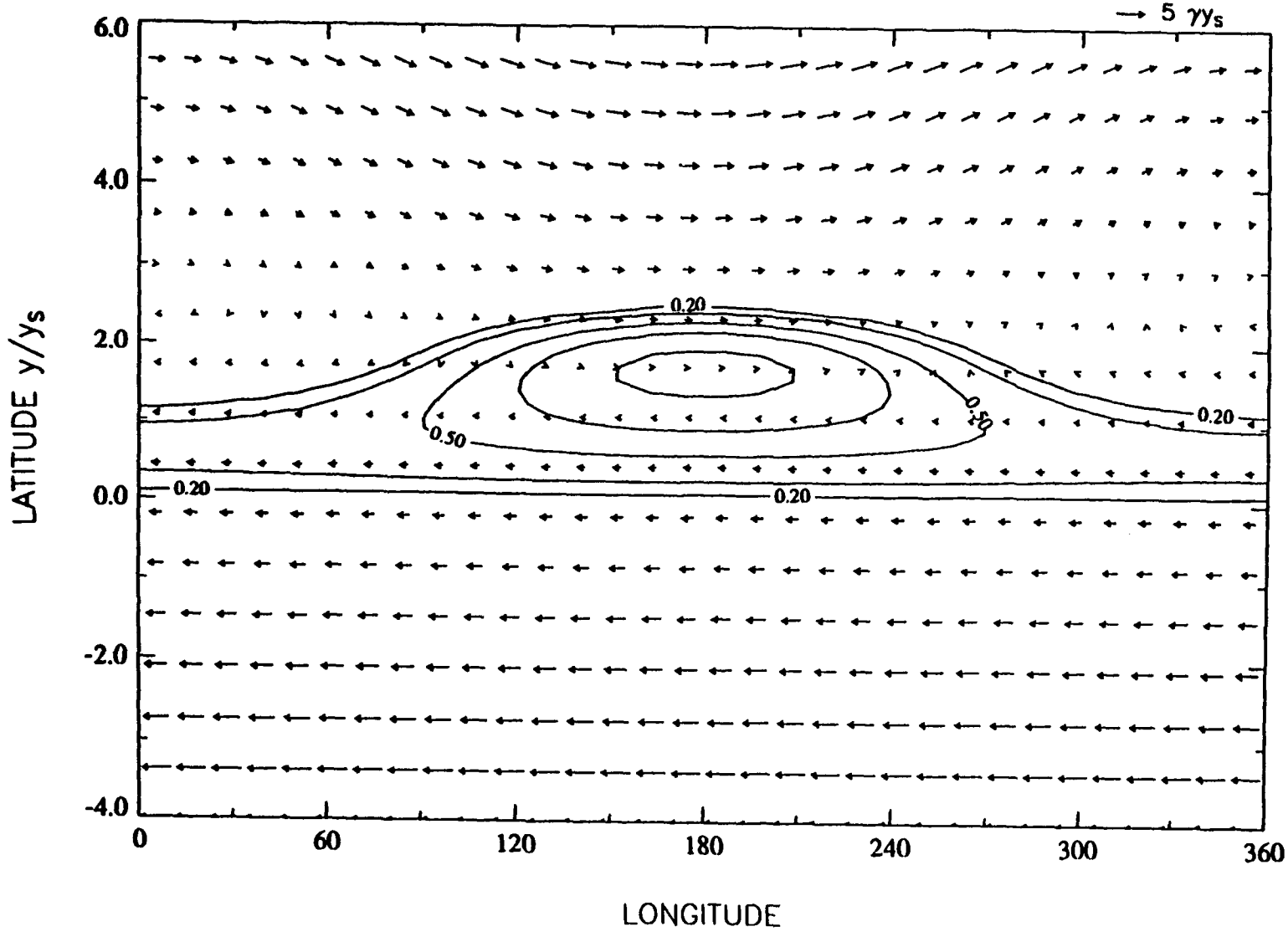

Fig. 2: Profile of nonparallel basic state (3.1) with $\psi = 1$. Contours show dimensionless parcel displacement growth rate R/γ. Contour interval 0.1, with 0.1 and 0.4 contours omitted.

This had a minor effect compared to the zonal component (3.1). Although the details are omitted, it can be stated that all of the results shown here were similar when $V \equiv 0$. Local instabilities were also found when $U \equiv 0$ and $V = V(x)$ (localization due to $\partial V/\partial x$). The effect of V was generally to disrupt rather than enhance the instability in comparison to parallel flow. These cases were felt to be less interesting and were not investigated further.

b. Latitude of maximum shear

The latitude of maximum latitudinal shear was y_c according to (3.1). On the other hand, the maximum rate of 'parcel instability' is $R \equiv \sqrt{-\beta y(\beta y + \varsigma)}$ where ς is relative vorticity. This quantity is contoured in Fig. 2; it did not always maximize at $y = y_c$ but was a function of y_c (and other parameters), having (for $\psi = 1$) an overall maximum value $R = 0.75\gamma$ when $y = y_c = 1.5y_s$. Maximum R was located north of y_s because the wave's contribution to basic state expanded the zone of instability at 180° (recall that y_s was the center of anomalous *zonal-mean* vorticity). However, as $|y_c| \to \infty$ the relative vorticity at $|y_c|$ became small relative to βy, so the region of anomalous vorticity next to the equator returned to a parallel configuration. For parallel flow the maximum $R = \gamma/2$ at $y = y_s$.

Growth rates of the most unstable mode as a function of y_c are shown in Fig. 3 for $\gamma = 4 \cdot 10^{-5}$ s^{-1}, $\epsilon^{-1} = 256$ m^{2}s^{-2}, $\psi = 1$, and $\bar{u}_0 = 0$. For these calculations 8 zonal harmonics were used, and $\Delta t = 900$ s. Vertical wavelength ~5 km for this choice of ϵ when $N = .02$s^{-1}. The asymptotic form of mode and growth rate were realized after a few days in most cases, although as will be seen later, this time scale depended on γ. The results appear reasonable: growth rate peaked at $y_c \approx 1.7y_s$ and for large $|y_c|$ instabilities developed as in parallel flow (not shown). However, the interpretation of Fig. 3 is slightly more complicated, because: (1) Instabilities near the center of the plot were exactly stationary ('s') and grew about twice as fast as in parallel flow – a larger variation than expected from R alone. Peak growth occurred a little to the right of $1.5y_s$. (2) Instabilities adjacent to those labeled 's' were zonally propagating but not global in extent.

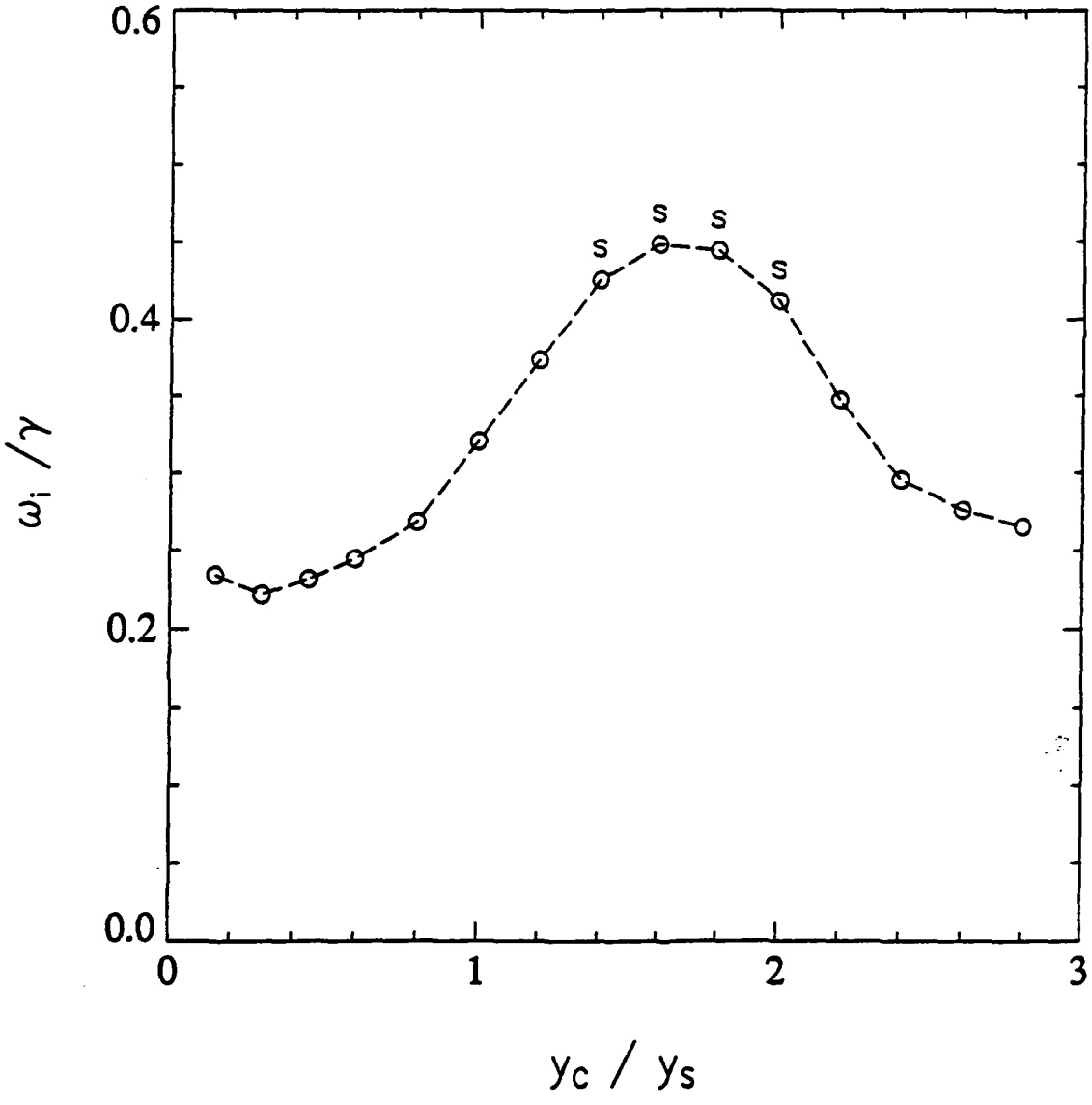

Fig. 3: Growth rate as a function of y_c. Local stationary instability denoted by 's'.

The basic state zonal flow $[\bar{u}(y) + U(x,y)$ in (3.1)] at location of maximum $R(180°, y)$ also varied with y_c; it was zero at this point when $y_c \approx 2.2y_s$. This variation affected the growth rate in addition to the variation of R. Growth was optimized for a combination that maximized R and minimized the *in situ* mean flow. The dependence of growth rate on mean flow speed, or breakdown of Galilean invariance, is characteristic of 'local' instability of nonparallel flow as discussed, e.g., by Pierrehumbert (1984). We return to this point in the next subsection and in Section 4.

Instability structure for $y_c = 1.8y_s$ is shown in Fig. 4. The disturbance was exactly stationary and confined to the middle half of the domain. Velocity was directed from low to high pressure indicating a dynamical source of instability (Coriolis force). Curiously the geopotential phase tilted slightly although no tilt was imposed on the basic state (3.1). Identical results were obtained with doubled resolution in x, y and $\Delta t = 450$ s.

Fig. 4 exemplifies 'local stationary' instability. Note, (1) although localized in x it is not infinitesimal in size. This indicates that terms in addition to $v'U_y$ are important in the dynamics, as expected from Section 2c. An oversimplified model could be formulated in which $v'U_y$ was the only term in A, all linear terms $\propto \partial/\partial x$ were dropped, and $B, C \equiv 0$. Growth rate in this case could be obtained from the symmetric formula (2.18a with $k = 0$) but was a function of x, implying a δ-function catastrophe. (This behavior was verified numerically.) (2) Absence of zonal propagation over a finite range of parameters (in this case, y_c) apparently requires the zonally symmetric ($s = 0$) component of perturbation, an important part of the total wave field. Most of the perturbation energy was contained in the lowest four harmonics. When the $s = 0$ component was artificially excluded from the numerical model, real phase speed was nonzero except where its trajectory crossed the $c_r = 0$ axis at a point near $y_c = 1.8y_s$.

In parallel flow, nonsymmetric instability propagates zonally except in the special case $c_r(k, \epsilon) \equiv -\bar{u}_0$ (Dunkerton, 1983; Stevens and Ciesielski, 1986). Only symmetric instability is trivially 'stationary' regardless of parameters. In nonparallel flow, local stationary instability is possible. It is in a sense 'locally symmetric' although this description ignores

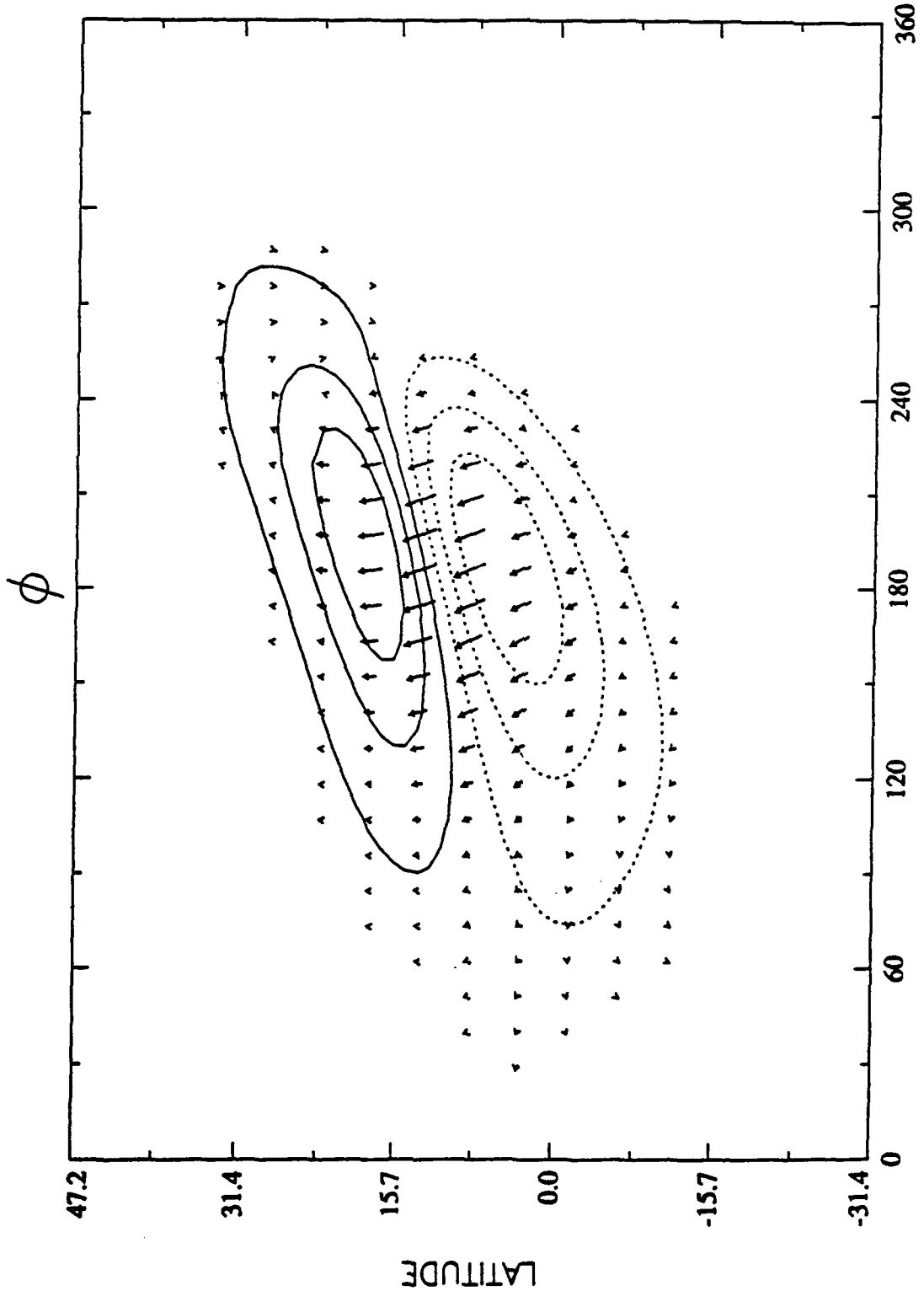

Fig. 4: Structure of local stationary mode for $\gamma = 4 \cdot 10^{-6}s^{-1}$, $\epsilon^{-1} = 256m^2s^{-2}$, $\psi = 1$, $\bar{u}_0 = 0$, and $y_s = 1.8y_s$. Negative ϕ-contours are dashed.

the spatial variation of instability structure (e.g., Fig. 4).

c. Dependence on $\bar{u}_0$

The term $\bar{u}_0$ in (3.1) added a constant mean flow independent of x, y. In parallel flow $\bar{u}_0$ would have no effect other than to shift phase speed by this constant. For local modes in nonparallel flow, growth rate is altered.

Fig. 5 shows ω_i/γ for the same parameters as Fig. 2 but with $y_c = 1.8y_s$ and $\bar{u}_0$ varied over a large range. Local stationary instability occurred near the point of zero mean flow, but for large $|\bar{u}_0|$, the instability was displaced off center and forced to propagate in the direction of $\bar{u}_0$.

An example of this zonally propagating or 'advected' instability is shown in Fig. 6 for $\bar{u}_0$ = -30 ms^{-1}. Propagation was to the west, and the pattern was observed to repeat every six days. Obviously this was insufficient time for global traverse, and in any case, the disturbance re-entering from the right had little role to play in the sequence.

It is generally thought that local instabilities belong to a class defined by 'absolute' instability (Pierrehumbert, 1984). Absolute instability is sensitive to a mean flow that displaces the center of mode away from the source of instability and thereby lowers the effective growth rate. When the mean flow is stable at large $|x|$, a sufficiently large $|\bar{u}_0|$ can stabilize the problem. This did not happen at the edges of Fig. 5 because of the zonally symmetric component of shear and periodic boundary conditions; advected modes simply wrapped around and continued to exist as 'global' modes in x, with smaller growth rate. A sponge region near $x = 0$, to simulate an infinite domain, dramatically altered the advected mode as discussed at the end of this section. The interpretation of local modes as absolute instability is deferred to the Appendix.

Of the two sub-types of local instability (stationary and advected), the stationary variety seems more relevant to equatorial Rossby-wave critical layers, for instance, when a

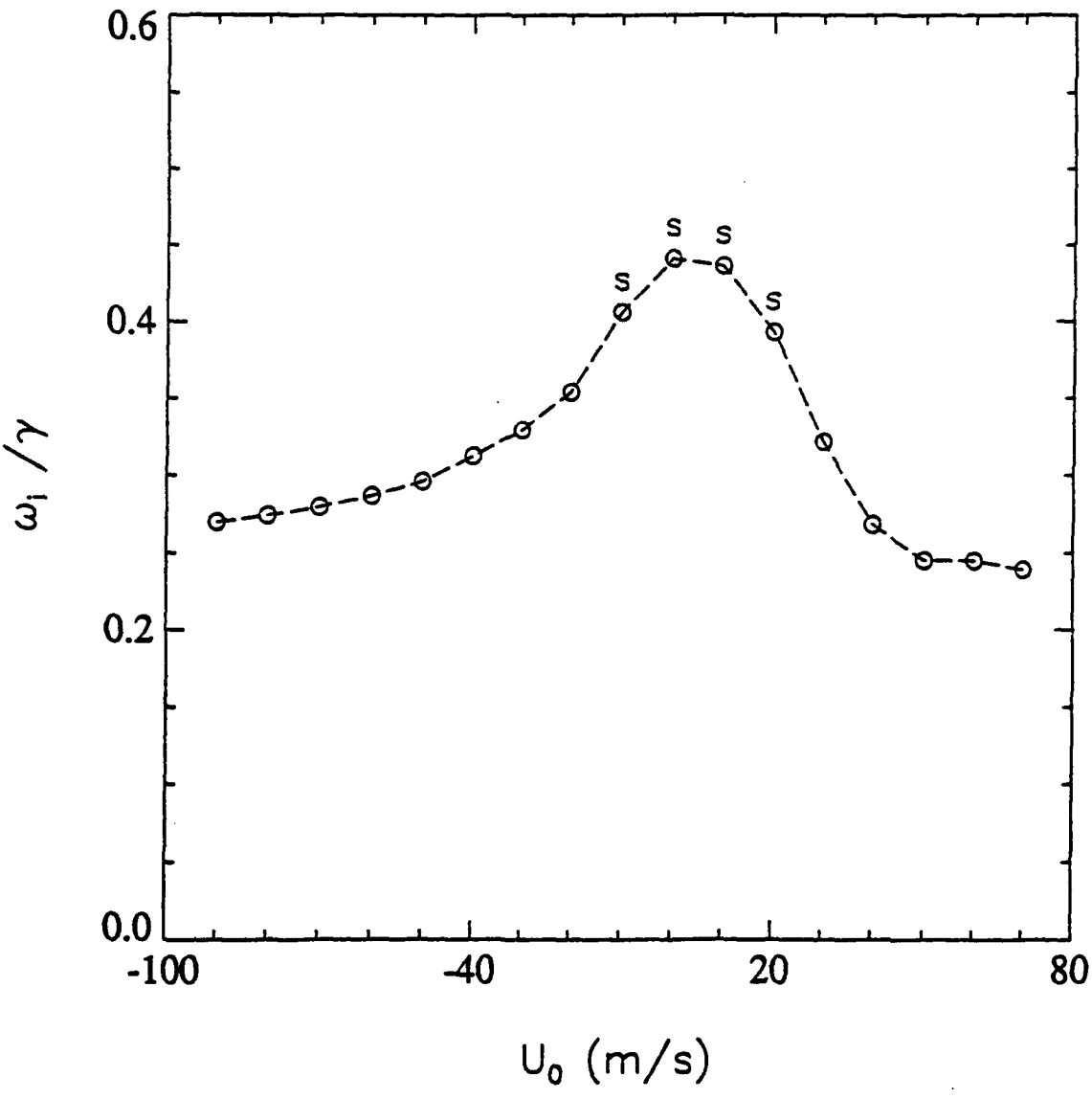

Fig. 5: Growth rate as a function of $\bar{u}_0$.

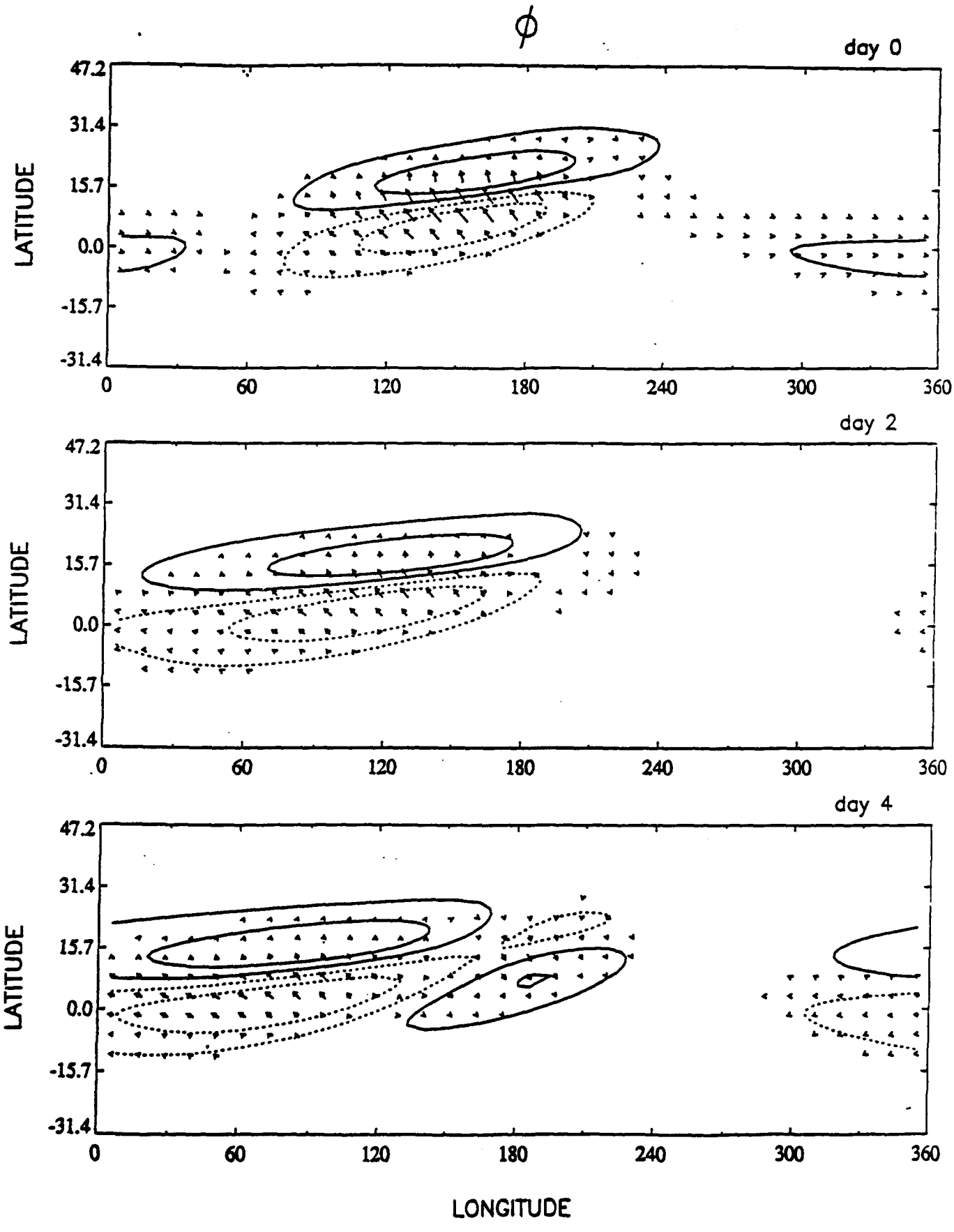

Fig. 6: Structure of unstable 'advected' mode for parameters of Fig. 4 but with $\bar{u}_0$ = -30 ms^{-1}.

quasi-stationary Rossby wave induces a region of significantly anomalous potential vorticity near the zero-wind line. Here the advecting mean flow is small. That is presumably why instabilities simulated by O'Sullivan and Hitchman (1992) were quasi-stationary ('locally symmetric') and followed the anomalous PV during critical layer development.

d. Transition to longitudinally 'global' instability

The value of ψ in (3.1) determined the zonal variation of shear. It was found to no surprise that as ψ decreased there was a transition to global instability, as shown in Fig. 7 ('p' signifying a globally propagating or parallel-flow instability). Growth rate was reduced as $\psi \rightarrow 0$. Parameters were the same as before, but with $y_c = 1.8y_s$, $\bar{u}_0 = 0$, and variable ψ. The structure became essentially that of nonsymmetric instability in parallel flow (Stevens and Ciesielski, 1986), with enhanced amplitude near the most unstable region (see Fig. 8, for $\psi = 0.2$). These were global modes that recycled through the entire domain. (Following Pierrehumbert, 'global' refers only to the *longitudinal* extent of eigenmodes.)

Results at very small ψ depended on initial conditions. A wavenumber 1 initial disturbance, used in most simulations here, produced wave 1 nonsymmetric instability. Initial wave 2 led to wave 2 instability at small ψ, with slightly larger growth rate. Wave 3 was near the short-wave cutoff and less unstable.

The time-dependent model simulated only the most unstable mode; however, we expect local and global modes of instability to coexist, at least in cases such as Fig. 2 where the flow is unstable at all x. Whether global modes of inertial instability are important in the middle atmosphere or anywhere else is uncertain.[2]

[2]There is an intriguing visible-light photograph of Jupiter taken by the Hubble Space Telescope on May 28, 1991 revealing horizontally-tilted, banded structures next to the equator (see, e.g., the cover page of AGU publication *Earth in Space*, January 1992 issue). This would suggest horizontally-divergent circulations perhaps due to a dynamical instability.

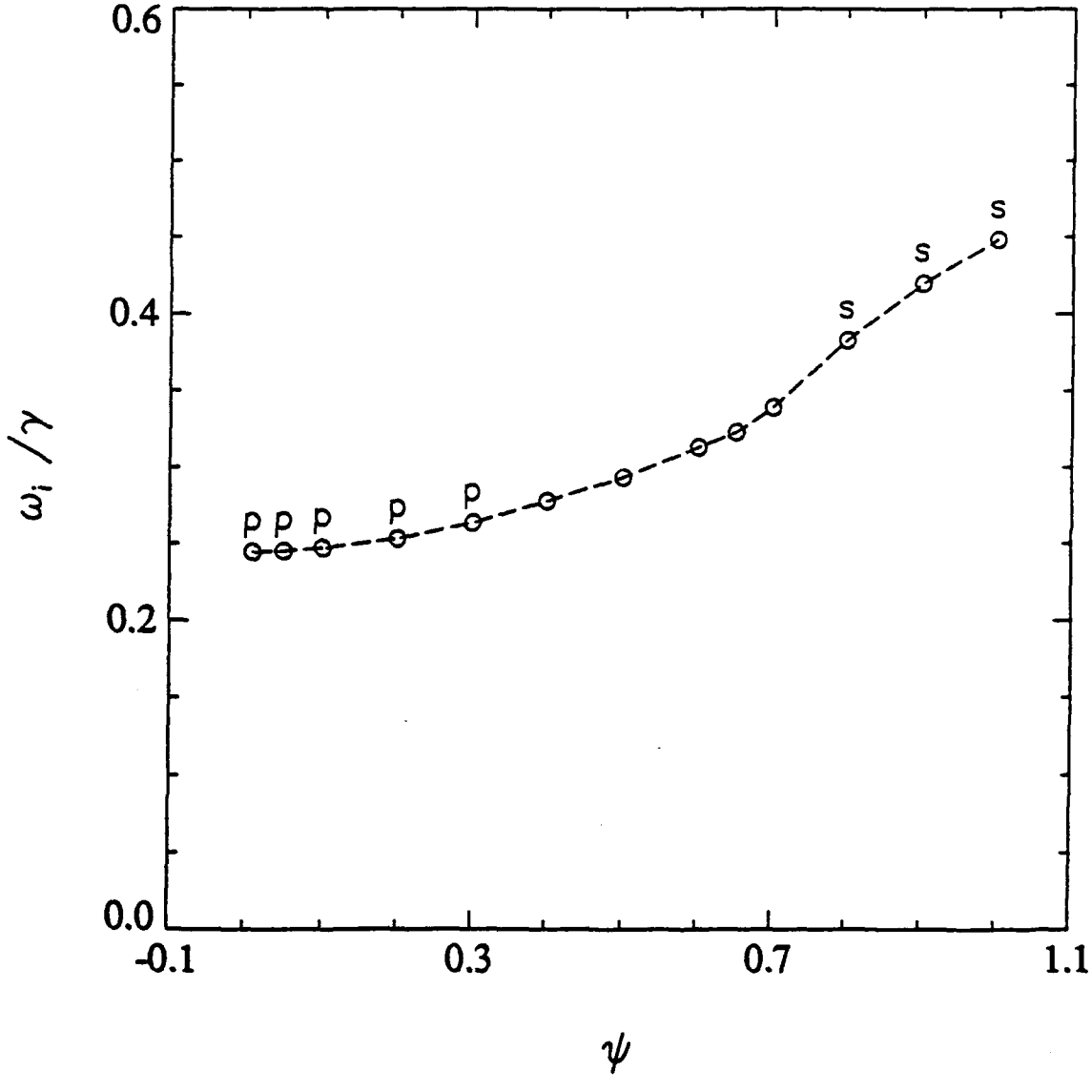

Fig. 7: Growth rate as a function of ψ. Globally propagating or parallel-flow instability denoted by 'p'.

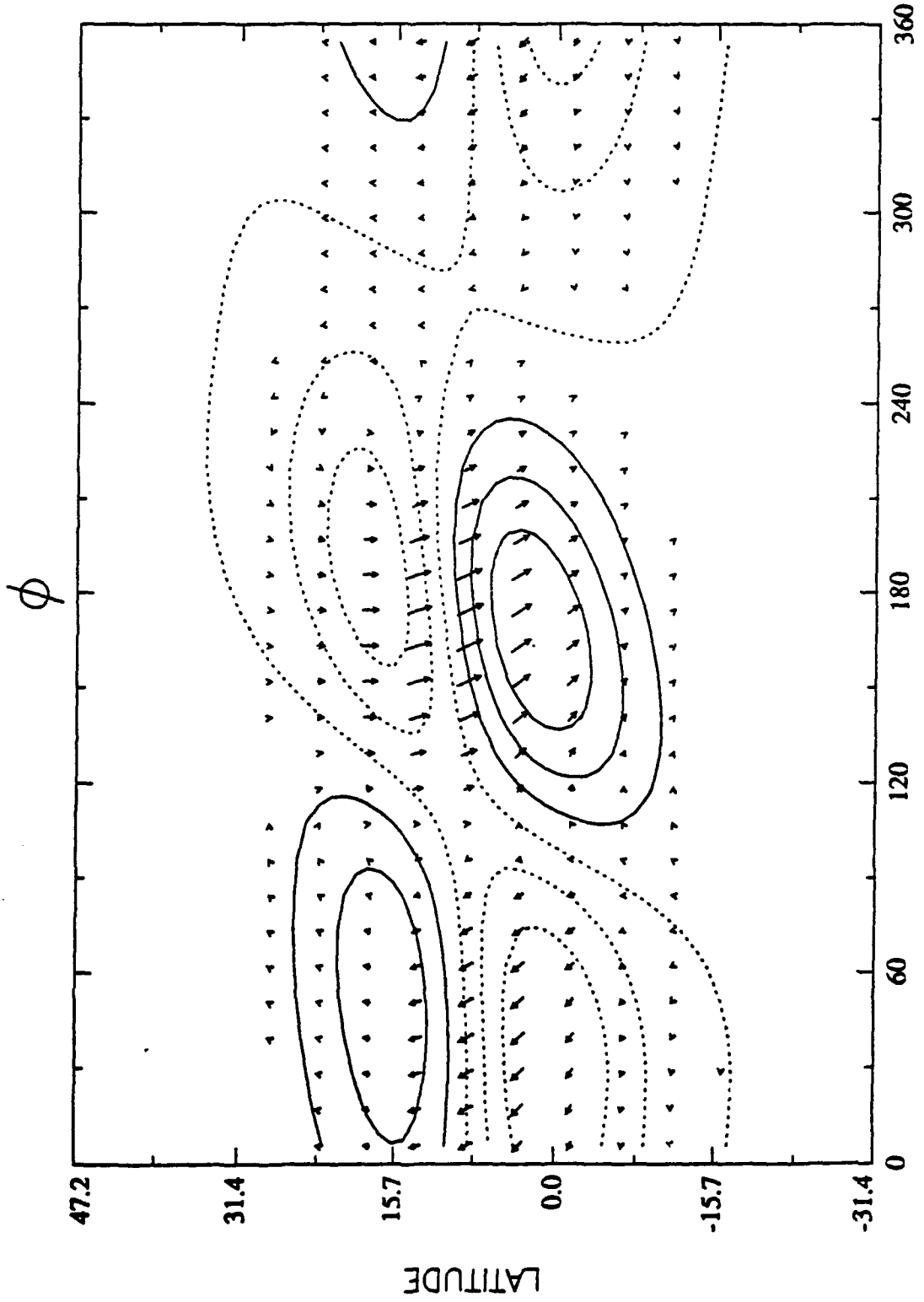

Fig. 8: Structure of global instability for parameters of Fig. 4 but with $\psi = 0.2$.

e. Variation of ϵ

The value of ϵ^{-1} in Figs. 3-8 (256 m^2s^{-2}) was near the neutral point $\epsilon_{neut}^{-1} = 305$ m^2s^{-2} for $\gamma = 4 \cdot 10^{-5}$ s^{-1}. Vertical wavelength was ~5 km when $N = .02s^{-1}$. [The reader may refer to (1.1) for other N, and recall the transformation of variables in Dunkerton (1983) allowing generalization to arbitrary values of shear.]

Recalling the discussion of Section 2c, the 'neutral point' limits symmetric instability in parallel flow. There is no *neutral curve* at small ϵ (except at small k adjacent to the neutral point: see Boyd and Christidis, 1982) to prevent instability at nonzero $s = ka$. For $\gamma = 4 \cdot 10^{-5}$ s^{-1}, several unstable integer wavenumbers are allowed below the short-wave cutoff (s = 0-3). Growth rate varies monotonically, increasing with ϵ to a limiting value $\gamma/2$ (cf. Fig. 1).

In nonparallel flow, the growth of local instability depended on ϵ in a similar way as shown in Fig. 9. The same parameters were used in (3.1) with $y_c = 1.8y_s$, $\psi = 1$, and $\bar{u}_0 = 0$. Growth rate varied monotonically, reaching a plateau at higher ϵ. Over most of this range the instability was stationary, displaying slow eastward propagation only at small ϵ. It seems clear from this example that nonparallel instability exists below the neutral point whether one adopts a 'zonal mean-flow' value ($\epsilon_{neut}^{-1} \sim 305$ m^2s^{-2}) or hypothetical 'local' value ($\epsilon_{neut}^{-1} \sim 1545$ m^2s^{-2}) at center of domain.

The structure of instability at small ϵ had several interesting features (not shown): the latitudinal scale was enlarged, as in classical equatorial wave theory, so instability extended into the stable part of the domain. Its structure resembled a Rossby wave in the northern hemisphere and eastward inertia-gravity wave in the southern hemisphere (Matsuno, 1966). The real phase speed, though slow eastward, was for practical purposes stationary with respect to the ground. The disturbance propagated, with respect to the fluid, westward north of the equator and eastward south of the equator. Because of latitudinal shear, a fused Rossby/inertia-gravity structure could be excited by equatorial instability that acted

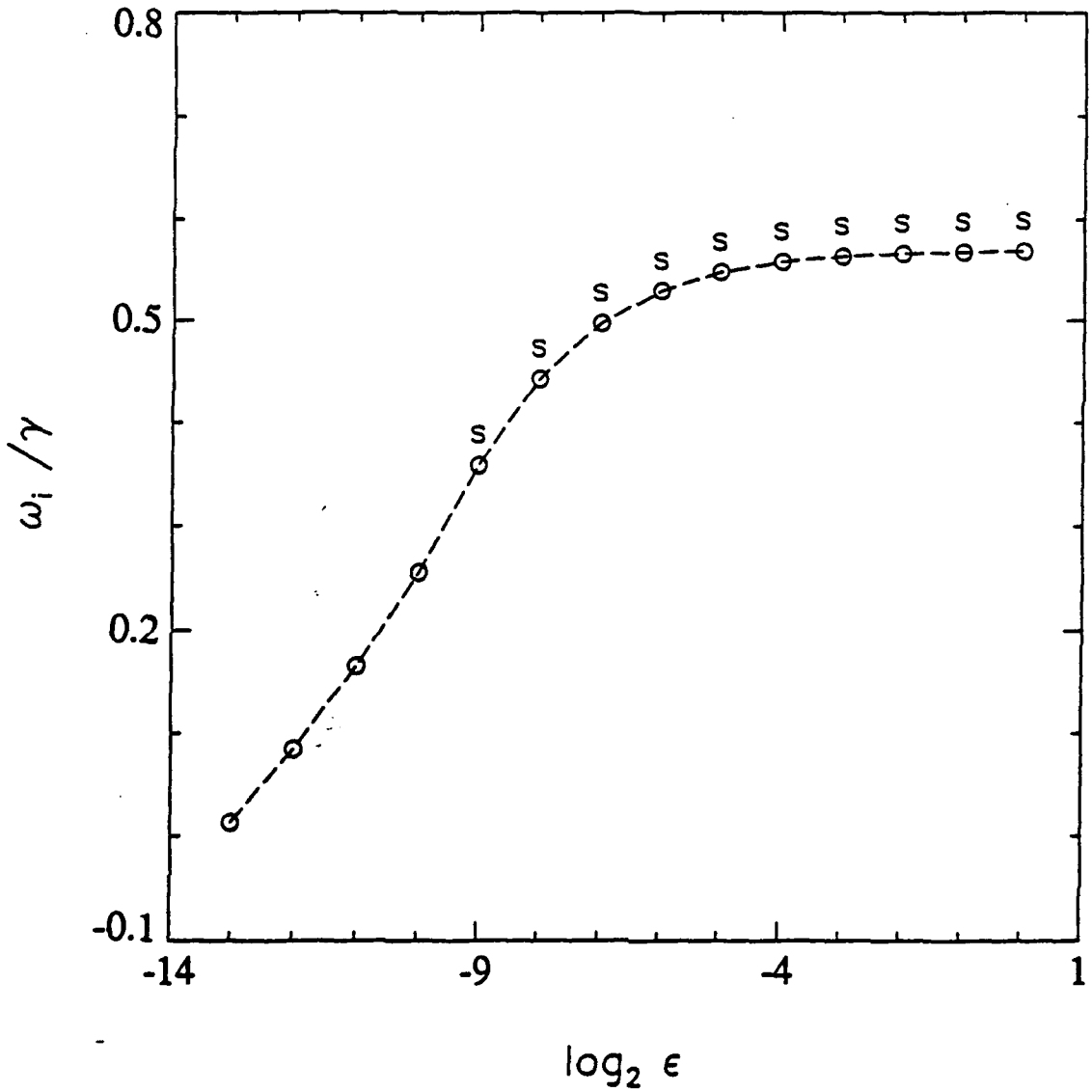

Fig. 9: Growth rate as a function of ϵ.

as a kind of 'wavemaker' in this instance.[3] The instability was, however, local in x.

The structure of instability at large ϵ resembled Fig. 4 but was contracted in latitude, remaining local in x.

Fig. 9 suggests that as in parallel flow, scale selection at finite $|m|$ is unrealized in the simple model. Dunkerton (1981, 1983) argued that vertical diffusion selects finite $|m|$. With diffusion there is a net growth rate $\omega_i^{\text{eff}} = \omega_i - \nu\epsilon N^2$. In the real world it is uncertain whether diffusion causes scale selection or is *a posteriori* caused by instability. (In the mesosphere, breaking internal gravity waves will help stabilize the flow.) Other factors may be important: (1) Stability depends on basic state transience; instabilities must grow rapidly compared to mean-flow change. In the tropical mesosphere, planetary waves will modify the basic state on a time scale of 1-5 days. (A Lagrangian time scale is what matters inasmuch as the basic state conserves potential vorticity on fluid parcels and inertial instability is to some extent a 'parcel' instability dependent on anomalous PV.) It would therefore be consistent to require $\gamma \geq 1\text{-}2\cdot10^{-5}$ s^{-1} for instability (cf. Hitchman and Leovy, 1986; Hitchman *et al*, 1987). (2) Realistic basic states contain a continuous spectrum of horizontal and vertical motions. The initial evolution need not be dominated by the most unstable mode, in fact the instability at finite amplitude need not be modal. (3) The meridional circulation itself has a weak stabilizing influence at large ϵ (Section 3f).

f. Effect of meridional circulation

Cross-equatorial shear in the middle atmosphere is due to diabatic advection by a mean meridional circulation. Including in (2.3) a zonally symmetric component $\bar{v}_0$, independent of latitude, had a minor effect on local stationary instability as shown in Fig. 10. For this series $\gamma = 4 \cdot 10^{-5}$ s^{-1}, $\epsilon^{-1} = 256$ m^{2}s^{-2}, $y_c = 1.8y_s$, $\psi = 1$, and $\bar{u}_0 = 0$. The location of instability was shifted north and east when $\bar{v}_0 > 0$ (not shown). Growth rate was slightly faster in most cases with $\epsilon^{-1} \geq 256$ m^{2}s^{-2} plotted in Figs. 3,5,7,9 when $\bar{v}_0 = 5$ ms^{-1}. At

[3]Frontal excitation of inertia-gravity waves in a localized region of conditional 'symmetric' instability was noted by Thorpe and Rotunno (1989) and Jones and Thorpe (1992).

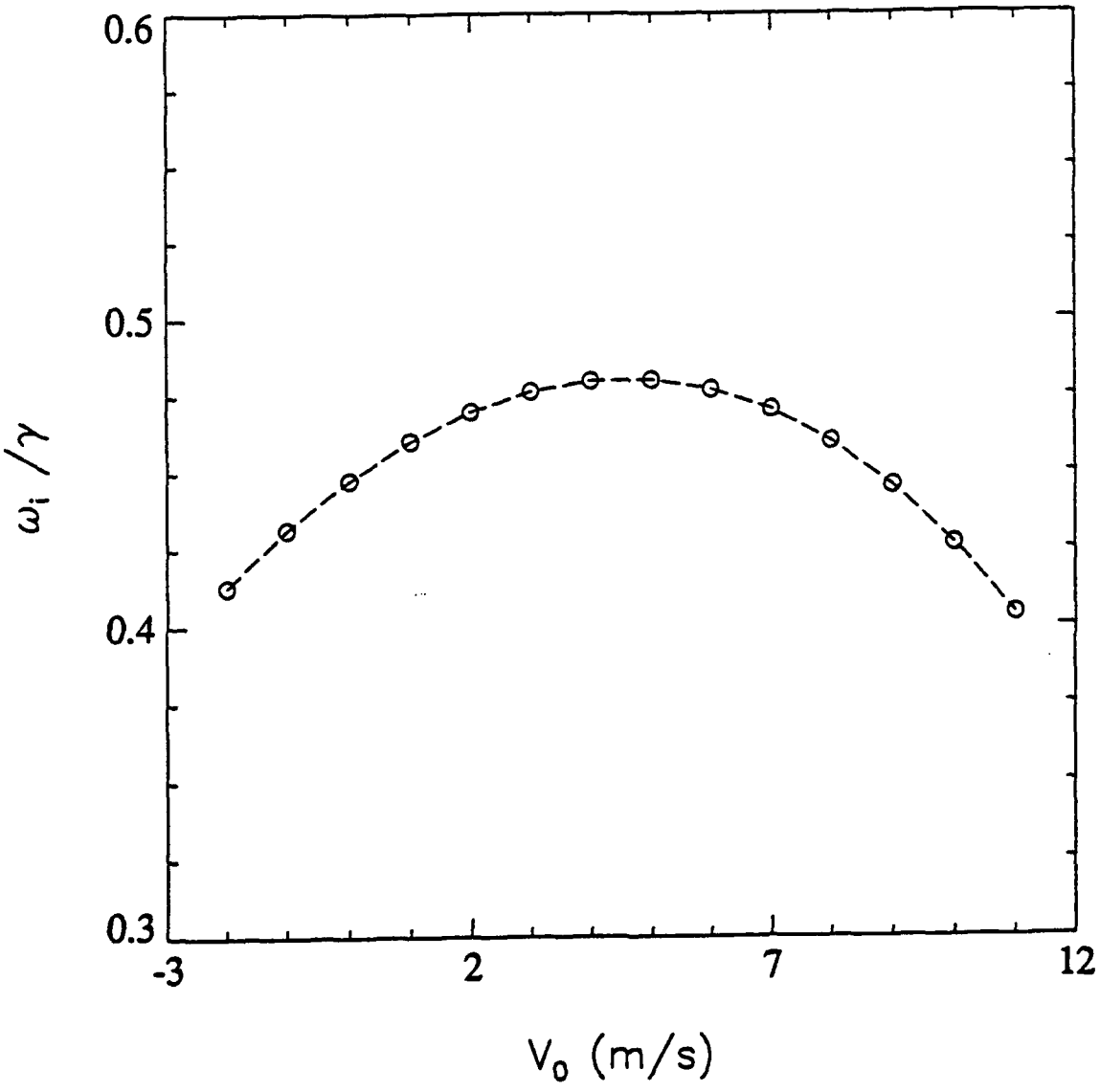

Fig. 10: Growth rate as a function of $\bar{v}_0$.

large ϵ there was a reduction of growth suggesting the possibility of weak scale selection when $\bar{v}_0 > 0$. The physical explanation may be that $\bar{v}_0$ advects the instability away from maximum R, the effect being more dramatic for high-ϵ modes with short meridional scale.

g. Results for weak shear

The preceding results raise two questions about instability in nonparallel flow. (1) Observe from Figs. 4,6 that local instability had the same zonal scale as basic state variation. There was at most one stationary or two propagating cells in the x-direction. In general, we expect multi-cell nonsymmetric instability in 'locally parallel' flow. Under what circumstances, then, can a wavetrain of many cells develop in the unstable part of the flow? (2) Advected instability was observed at large $|\bar{u}_0|$ because the flow was unstable at all x and periodic boundary conditions were assumed. Real flows could be stable at some longitude. Is advected instability possible in this case? The first question will be addressed now and the second in the next subsection.

It was seen in parallel flow that the minimum zonal scale for latitudinal trapping of eigenfunctions (decay at large $|y|$) is defined by a short-wave cutoff $k_{\max}\gamma = \beta$. The argument could be extended to nonparallel flow; minimum zonal scale depends on shear. In the case illustrated above, it was impossible to accomodate several cells in the x-direction. For multiple cells γ must be reduced.[4]

Fig. 11 shows an example in which $\gamma = 0.5{\cdot}10^{-5}\ \mathrm{s}^{-1}$, $\epsilon = 4\ \mathrm{m}^{-2}\mathrm{s}^2$, $y_c = 1.8y_s$, $\psi = 1$, and $\bar{u}_0 = 0$. Numerical integration used 32 harmonics (note change of axes); results are shown at 240 days. For this value of γ a long time was required to obtain the mode, due to the assumed γ and wave 1 initial condition. (Less time would have been required from high-k initial conditions.) This example demonstrated that multi-cell instability is possible when the characteristic scale of mean-flow variation is much greater than $k_{\max}^{-1} \equiv \gamma/\beta$. Another

[4]That is, in the configuration (3.1). There may exist situations where γ is unimportant outside the region of anomalous PV, such that trapping of eigenfunctions is ensured by the basic state alone, apart from k.

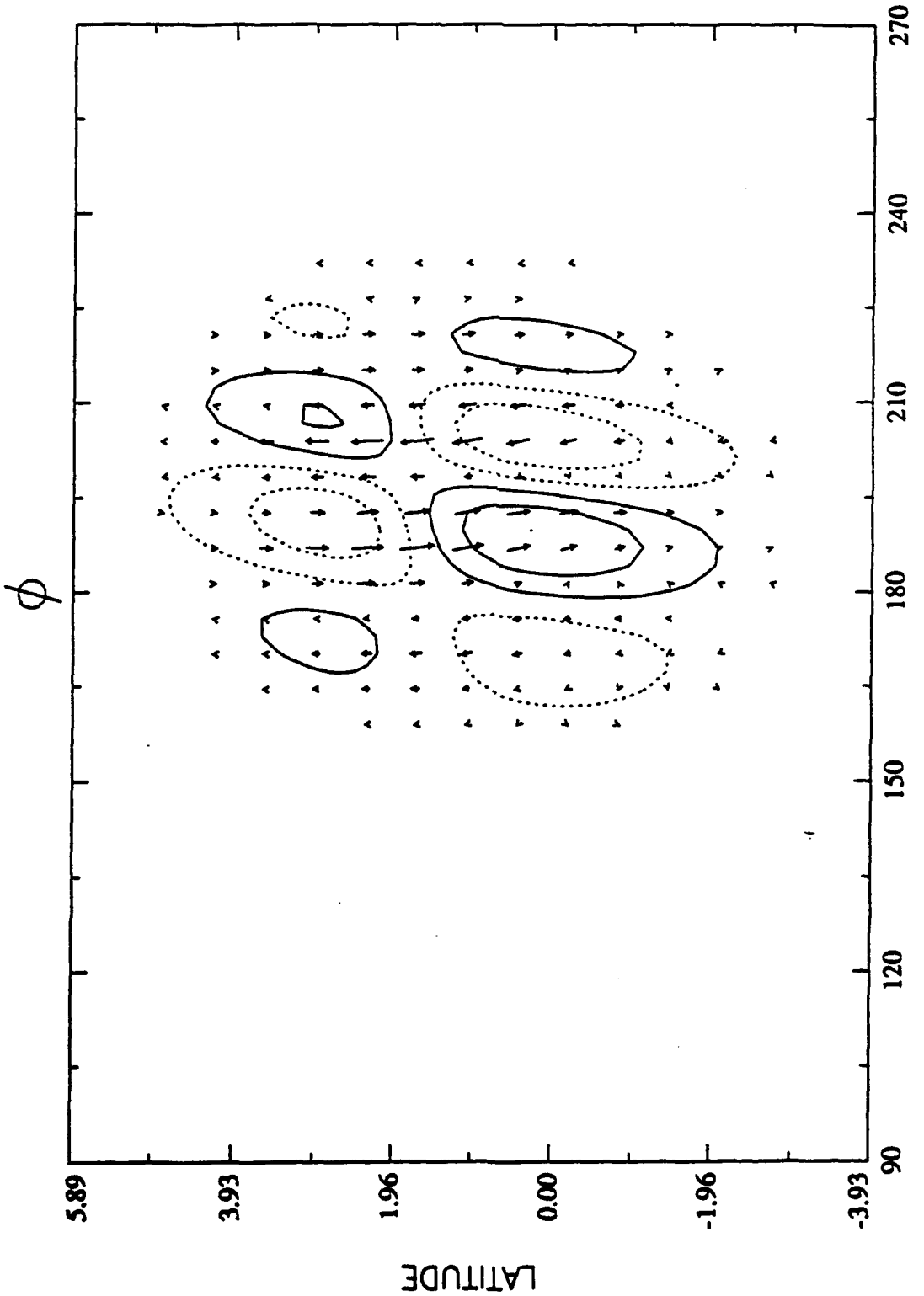

Fig. 11: Structure of multi-cell instability in weak shear $\gamma = 0.5 \cdot 10^{-5} s^{-1}$.

example of small γ is discussed in the Appendix.

What about the opposite situation, when the unstable region is smaller than k_{max}^{-1}? Profiles of the form (3.1) could be generalized in order to confine the most unstable flow:

$$-\cos(x/a) = 2\sin^2(x/2a) - 1 \rightarrow 2\sin^n(x/2a) - 1 \tag{3.3}$$

Setting $n = 16$, for example, the region of most unstable flow was less than 60° wide. Results indicated that, for parameters of Fig. 4, the local stationary mode was essentially unchanged by reducing the size of unstable region, although growth rate was reduced slightly (by about 25% when $n = 16$). (An explicit version of the time-dependent code was used to obtain this result and to validate other results of the semi-implicit model.) This supports its interpretation as a local mode that depends, not on global average stability, but local stability within the most unstable part of the domain (Pierrehumbert, 1984).

To be sure, the concept of 'local stability' is imprecise when (as in this case) instability and basic state share the same zonal scale. WKB analysis like that of Pierrehumbert (1984) is formally valid only in slowly varying mean flow. Perhaps a more accurate measure of stability would be obtained by averaging, say, over a half-wavelength of perturbation.

h. Sponge region in x

As mentioned in Section 2c the advected instability was altered by a sponge region designed to completely absorb disturbances crossing the domain boundary near $x = 0$. Though artificial, the sponge may simulate regions of stable flow (as undoubtedly exist in the atmosphere) or the tendency of instabilities to 'break' and dissipate through nonlinear saturation before making a complete circuit of the globe.

Fig. 12 shows growth rate as in Fig. 5 but with sponge region included. Instabilities were unaffected at small $|\bar{u}_0|$ but were stabilized at large $|\bar{u}_0|$. The physical interpretation is that $\bar{u}_0$ displaced the center of mode downstream from the source of instability near x = 180°. For sufficiently large $|\bar{u}_0|$ the mode was pushed into the sponge region and could

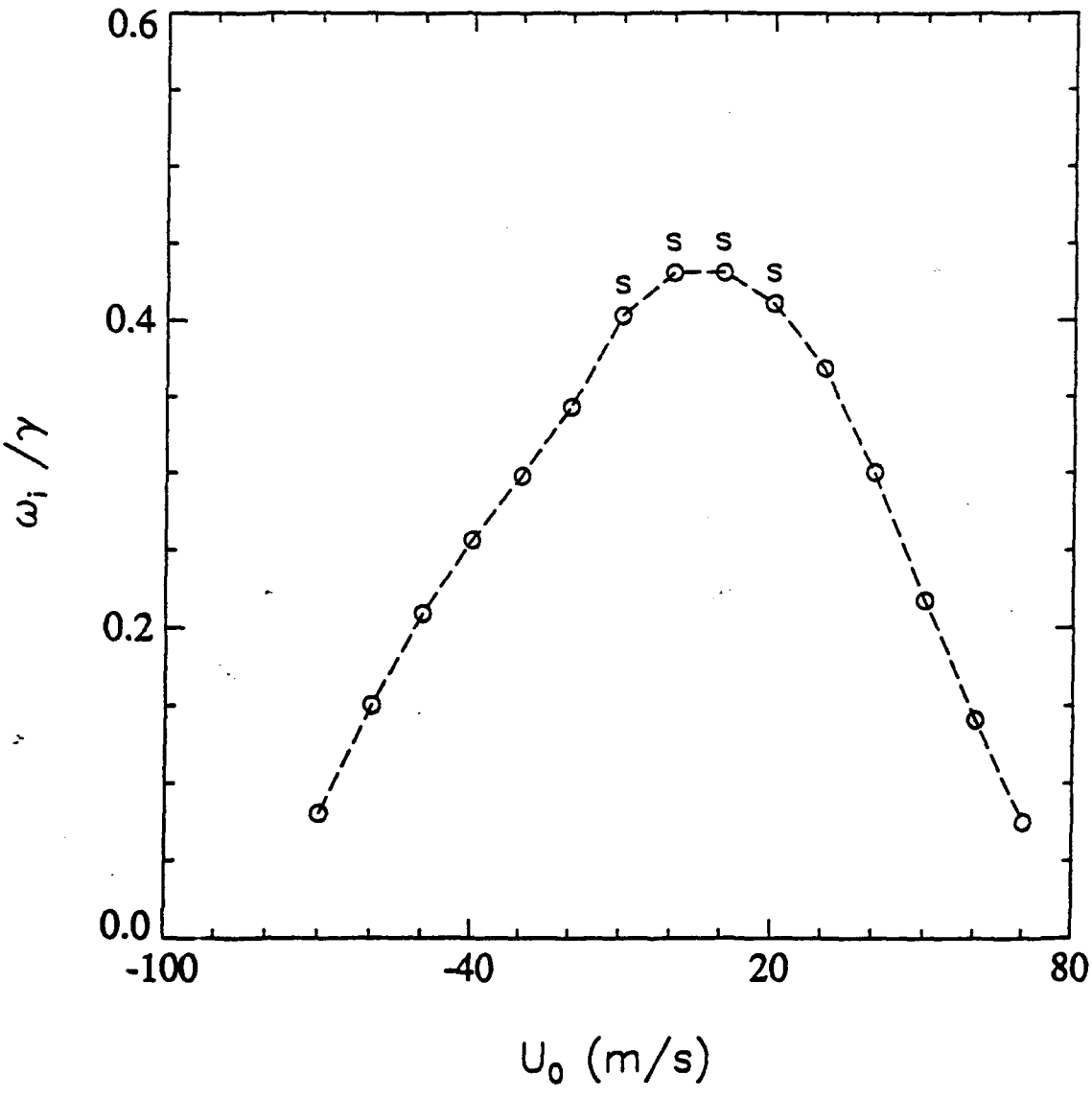

Fig. 12: Growth rate as a function of $\bar{u}_0$ as in Fig. 5, but with sponge region included.

not grow. Evidently 'global' modes were stabilized by the sponge region also.

4. Discussion

Results of Section 3 documented local as well as global modes of inertial instability in nonparallel flow. Local modes dominate inhomogeneous flow and are likely more important in observed basic states. Local stationary instabilities had the largest growth rate, depending primarily on the local rather than global stability of the basic state; they occurred when (among other things) mean flow advection was small in the unstable region. Large advection caused zonal phase propagation, here referred to as advected instability. Like stationary modes, advected modes had zero group velocity but the center of wave packet was displaced downstream from the most unstable longitude, and the growth rate reduced. If $\bar{u}_0$ was sufficiently large and the flow stable at large $|x|$, advected modes were stabilized.

Even for a simple profile like (3.1) the parameter dependence of inertial instability is complicated; examples of Section 3 highlighted behavior along a few trajectories in parameter space. One of the more interesting results was the dependence of local instability on $\bar{u}_0$, illustrating the breakdown of Galilean invariance in nonparallel flow. Zonal inhomogeneity breaks the symmetry of uniform parallel flow and introduces a new constant: the zonal propagation speed of basic-state pattern. This was zero in (3.1); consequently, instabilities with zero group velocity remained in the same location relative to the mean flow pattern at all times. (Not surprisingly their growth maximized when the mode best overlapped the most unstable region.) In WKB theory, a flow is said to be ***absolutely unstable*** when such instabilities exist, i.e.

$$\omega_i(k_0) > 0 \tag{4.1}$$

where

$$\left.\frac{\partial \omega}{\partial k}\right|_{k_0} \equiv 0 \tag{4.2}$$

and unstable branches originate on opposite sides of the real-k axis (e.g., Pierrehumbert, 1984, 1986). The importance of absolute instability derives from symmetry-breaking, e.g., in nonparallel/nonuniform flow, or when there is a 'wavemaker' at some x (Huerre and Monkewitz, 1990).

Pierrehumbert (1984) analyzed the two-layer quasi-geostrophic model for baroclinic instability of nonparallel flow, including a discussion of 'absolute' and 'convective' instability in terms of local and global modes, supplemented by WKB analysis. It is unnecessary to duplicate this work, but simpler to quote three of his main conclusions pertaining to local modes:

1) *Growth rate of a local mode is determined by the maximum baroclinicity in the domain, and not by the average baroclinicity.*

This was suggested for inertially unstable flow (substituting 'inertial instability' for 'baroclinicity') by results of Figs. 5,12 demonstrating the insensitivity of local stationary instability to a sponge region near $x = 0$, and by discussion at the end of Section 3g in which growth rate was only weakly dependent on the size of the unstable region. As in Pierrehumbert (1984) the 'maximum baroclinicity' or 'maximum inertial instability' of the basic state must take into account factors (such as boundary conditions, pressure gradients, and $\bar{u}_0$) in addition to the parcel growth rate (e.g., R). On this account we are reminded that equatorial inertial instability is not a pure 'parcel' instability (Dunkerton, 1983).

2) *Vanishing absolute growth rate at infinity is not necessary for localization.*

This was apparent from examples based on the profile (3.1) which was unstable at all x but displayed a preference for local instabilities in most circumstances.

3) *The contrast between maximum and minimum baroclinicity in the flow determines the extent of localization of the eigenmodes, with high contrast favoring localization.*

In a similar way (although it was not discussed extensively above), the zonal scale of local instability increased as ψ was decreased below 1, before the onset of global instability.

Absolute instability does not depend on the validity of WKB in (4.1,2) since, by definition, the instability must grow indefinitely at a fixed point in x. This property was demonstrated numerically, but not analytically, for local stationary instability. WKB analysis of inertial instability on an equatorial beta-plane is difficult although suggestive of absolute instability as discussed in the Appendix. Basic states like Fig. 2 disallow a clean separation of wave and mean-flow scales, and a numerical demonstration of instability is preferable in this case (cf. Jones and Thorpe, 1992).

5. Conclusion

Using a simple model it was shown that inertial instabilities in zonally nonuniform cross-equatorial shear take the form of local and global modes. Local modes may be exactly stationary or display zonal phase propagation depending on, among other things, advection by the basic state. Both sub-types of local instability are distinguished from global instability by their zero group velocity and concentration of amplitude within, or downstream from, the region of most unstable flow. These properties, including breakdown of Galilean invariance, are reminiscent of 'absolute' instability – although, apart from the Appendix, none of our results depended on a WKB approximation. Exact stationarity of phase over a finite range of parameters, and measurable dependence of growth rate on the size of unstable region, are possibly attributable to a non-WKB effect.

It was suggested that for equatorial Rossby-wave critical layers in the mesosphere, local stationary modes are important given the strength of background shear γ and weakness of *in situ* advecting current near the zero-wind line. Such a simplification is desirable in this context to avoid the complexity of global and advected modes. Existence of local stationary modes locked to PV anomalies is consistent with middle atmosphere simulations of inertial instability and Rossby wavebreaking by O'Sullivan and Hitchman (1992). As a follow-up it will be worthwhile to show the evolution of unstable modes in an authentic Rossby wave critical layer, and their effect on potential vorticity evolution. This will be done in the sequel.

Local and global modes of inertial instability share many of the same properties, e.g., dependence of growth rate on vertical wavelength, and downgradient momentum flux. Vertical scale selection may be achieved with diffusion as argued previously, or as the new analysis suggests, through mean meridional advection. Non-modal instability (Farrell, 1982) on a transient basic state will also allow scale selection at finite amplitude. It should be obvious from our results that when the time scale of basic state variation is much less than γ^{-1}, exponential modes of inertial instability are largely irrelevant.

Inertial instability can be expected to have three consequences in the tropical middle atmosphere: horizontal redistribution of angular momentum (and potential vorticity), dissipation of laterally propagating Rossby waves, and vertical mixing of constituents. Because of their similarity, local and global modes may contribute alike to mean-flow effects, such as inertial adjustment (Dunkerton, 1981) and mixing. (The efficiency of inertial adjustment is open to question. Our recent numerical results in the middle atmosphere demonstrate that an adjustment occurs but is incomplete. See also Thorpe and Rotunno, 1989 for further discussion in the context of frontal CSI.) Local modes will be more important for Rossby wave dissipation. According to Killworth and McIntyre (1985), barotropic processes are insufficient for time-averaged critical layer absorption as $t \to \infty$.

APPENDIX

Dispersion relation at complex k

Analysis of absolute instability in multi-dimensional flow is difficult; a formal proof of absolute equatorial inertial instability using WKB theory has not been given and will not be attempted here. (I doubt whether such a proof is possible for equatorial instability without approximation to the governing equations). It is interesting nevertheless to calculate eigenfrequencies of (2.10) at complex k. Several limitations of this approach should be noted. (1) Analysis begins with the complex dispersion relation defined numerically by (2.10) with $D = 0$ rather than the Laplace transform of the time-dependent system; this excludes continuum modes which may be important in reality. (2) The exact dispersion relation is determined numerically over a finite range of k, rather than analytically over all k. The cubic approximation of Section 2c (and a quadratic version of it) gave similar results, but their validity could not be guaranteed for all combinations ϵ, k. (3) The infinite beta-plane could not be simulated; results were obtained in a channel. Channel-dependent modes occur outside the short-wave cutoff (defined by a hyperbola in the complex-k plane extending outward from k_{max} on the real axis). This region will be ignored. (4) Construction of WKB solutions in some cases may require matching across a WKB breakdown point (Pierrehumbert, 1984); the full construction will not be attempted but it will be assumed that matching is possible.

To simplify matters, the shear was assumed independent of latitude:

$$\tilde{U} = \gamma(y - y_c)\left[\frac{1 - \psi\cos x/a}{1 + \psi}\right] \equiv \gamma(y - y_c)\Psi_f(x)$$

and $\tilde{V} \equiv 0$, corresponding as closely as possible to the theoretical results of Section 2c. Local stationary instability exists near $y_c = y_s$; discussion will center around this choice of y_s. The eigenproblem (2.10) was solved at $x/a = \pi$, the location of maximum shear (where $\Psi_f = 1$), allowing k to be complex. Eigenfrequencies were obtained by a shooting method for several combinations γ, ϵ. Results shown in Fig. 13 were representative when $\epsilon \sim \epsilon_{neut}$ (in this case, $\gamma = 1.5 \cdot 10^{-5}\text{s}^{-1}$, $\epsilon = 0.1657\ \text{m}^{-2}\text{s}^2$). Growth rate increased in both

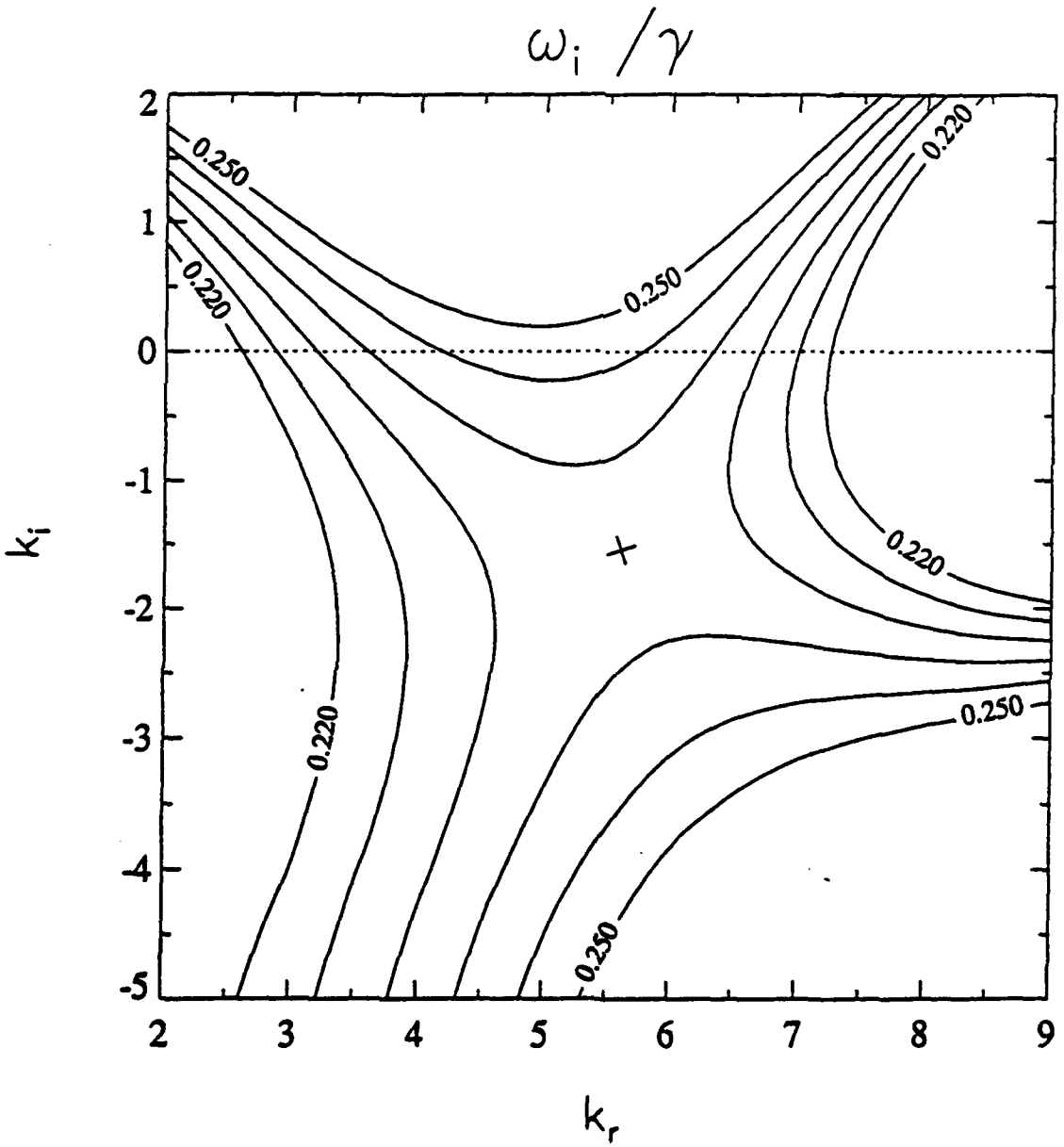

Fig. 13: Inviscid growth rate as a function of complex k obtained from the eigenproblem (2.10) with $D = 0$, $\pi = \gamma(y - y_e)$, $\gamma = 1.5 \cdot 10^{-5} s^{-1}$, $\epsilon = 0.1657\ m^{-2}s^2$, and $y_e = y_e$.

directions away from the real axis, and there was a saddle point near $s = ka = (5.55,-1.50)$ – not far from the 'most unstable wavenumber' on the real axis. Existence and location of the saddle are a function of parameters (γ, ϵ, Ψ_f, y_c, etc.) so there is nothing special about this example. In the inversion of Laplace transform, the saddle is considered 'unavoidable' when integrating over k_r if unstable branches originate on opposite sides of the real-k axis (Pierrehumbert, 1986). This was apparently the case based on numerical results, but an analytical proof is beyond the scope of this paper.

Not all saddles are unavoidable in this problem, particularly those on the imaginary axis resulting from merger of unstable branches originating in the upper half-plane. This sort of behavior was observed when $\bar{u} = \gamma y$.

Knowledge of $\hat{\omega}(k)$ is sufficient to determine new eigenfrequencies $\omega(k)$ from a complex Doppler shift

$$\omega(k) = \hat{\omega}(k) + k\bar{u}_0$$

where $\hat{\omega}$ is given by the complex dispersion relation in the 'control' case $y_c = y_s$ (e.g., Fig. 13). Other effects could be added, such as x-diffusion. In WKB theory, breakdown of Galilean invariance is evidently due to the imaginary part of k, as can be seen by translating a wave packet of exponential shape to the left or right. For constant shear, variation of y_c introduces a constant mean flow change $\bar{u}_0 = -\gamma\delta y_c \Psi_f$. The location of saddle point and its associated eigenfrequency change as a function of y_c; this is illustrated in Fig. 14 where comparison is made to time-dependent model results obtained with $\psi = 0.25$. The agreement is rather good. Growth maximized when the mean flow was zero near the center of the unstable region. Due to noticeable asymmetry of $\hat{\omega}(k)$ between upper and lower half-planes, results were not exactly symmetric about $y_c/y_s = 1.0$.

Growth rates were slightly smaller in the time-dependent model, by a few percent – possibly due to y-diffusion, included in the time-dependent model but not in the eigenproblem (2.10). (Horizontal diffusivity in the time-dependent model was approximately $2.1 \cdot 10^5 \mathrm{m^2 s^{-1}}$. Saddle-point values in Fig. 14 were corrected for x-diffusion only.) There was also a non-WKB effect such that growth rates in the time-dependent model diminished

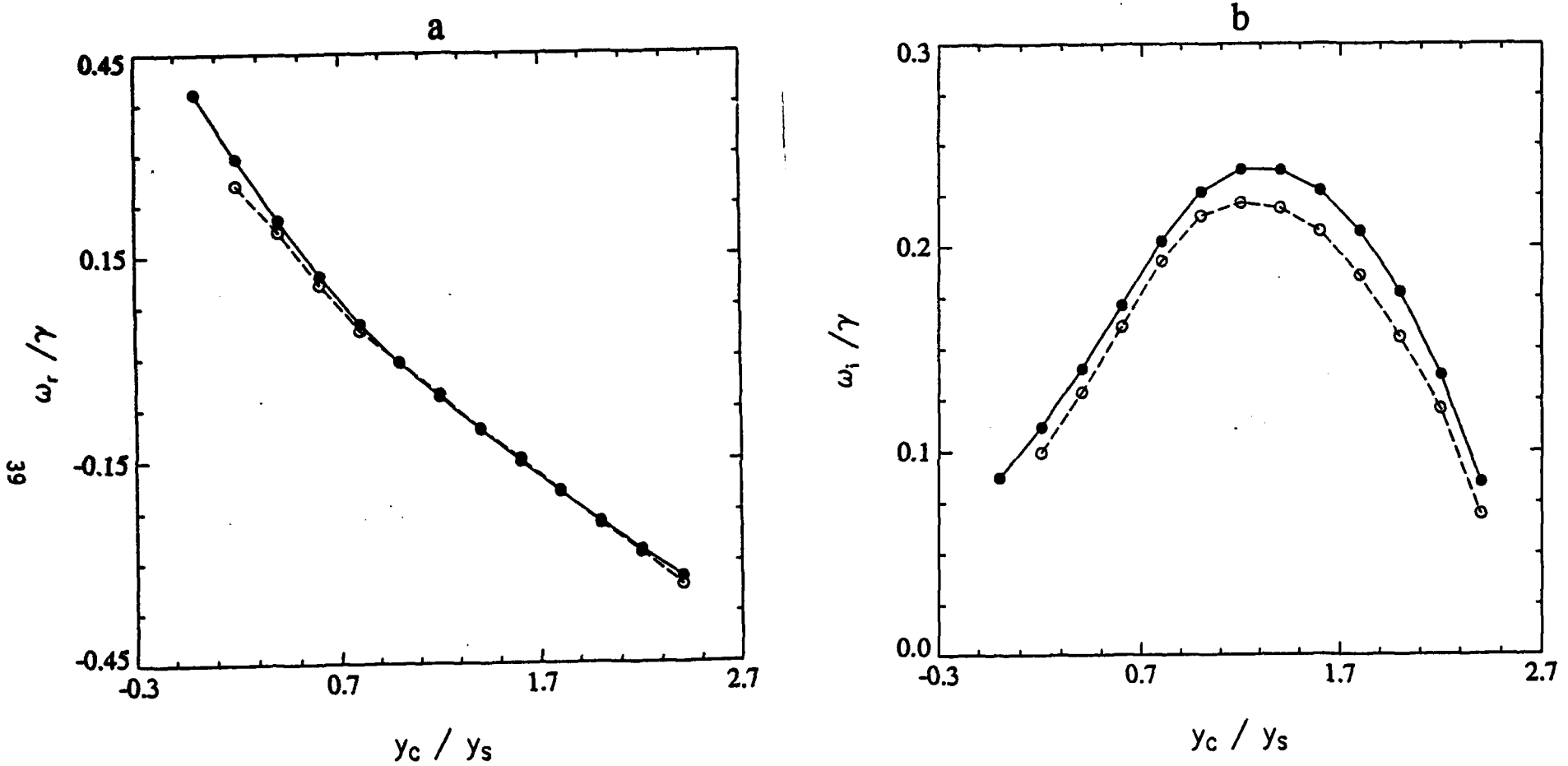

Fig. 14: Frequency (a) and growth rate (b) of local instabilities simulated in time-dependent model (dashed) compared with saddle-point values (solid).

as ψ increased, i.e., as the size of the unstable region was reduced in x. Simulations with $\psi \geq 0.25$ underestimated the true growth rate somewhat.

Calculated and observed periods were in reasonable agreement for 'advected' instabilities. Note that, unlike the situation in Fig. 3, ω_r was nonzero everywhere except near $y_c/y_s = 1.0$; this was due to the smaller value of γ and relatively smaller contribution from the zonally symmetric component of instability.

Displacement of the saddle point off the real axis implies growth of the wave packet between $x/a = \pi$ and its center which is displaced, in physical space, *downstream* from the region of most unstable flow. This expectation was verified by numerical results, including a more subtle prediction that zonal wavelengths are slightly larger (smaller) for packets displaced to the left (right) of center.

Finally, it was possible to vary x/a, holding other parameters fixed, and determine $k(\omega, x)$ with ω set equal to its saddle-point value as in Fig. 10 of Pierrehumbert (1984). This was a tedious calculation due to rapid variation of k; only two examples were attempted, one at ϵ_{neut}, and another above. In both cases, it was striking how quickly k departed from the real axis in both directions as Ψ_f was reduced below unity, which may help explain the 'locally symmetric' appearance of local instability having few cells in the x-direction. Also, it may explain why local modes can be found in weakly inhomogeneous flow, as only a slight reduction of Ψ_f below unity immediately moves k into the opposite half-plane – a necessary condition for the existence of local modes (Pierrehumbert, 1984).

When $\epsilon >> \epsilon_{neut}$, the saddle-point trajectory is closer to the imaginary axis, consistent with numerical results demonstrating the preference for quasi-stationary, single-cell instability in this case.

REFERENCES

Andrews, D.G., and M.E. McIntyre, 1976: Planetary waves in horizontal and vertical shear: the generalized Eliassen-Palm relation and the mean zonal acceleration. *J. Atmos. Sci., 33*, 2031-2048.

Andrews, D.G., J.R. Holton, and C.B. Leovy, 1987: *Middle Atmosphere Dynamics*. Academic Press, 489 pp.

Bennetts, D.A., and B.J. Hoskins, 1979: Conditional symmetric instability – a possible explanation for frontal rainbands. *Quart. J. Roy. Meteor. Soc., 105*, 945-962.

Boyd, J.P., 1978: The effects of latitudinal shear on equatorial waves, Part 1: theory and methods. *J. Atmos. Sci., 35*, 2236-2258.

Boyd, J.P., and Z.D. Christidis, 1982: Low-wavenumber instability on the equatorial beta-plane. *Geophys. Res. Lett., 9*, 769-772.

Ciesielski, P.E., D.E. Stevens, R.H. Johnson, and K.R. Dean, 1989: Observational evidence for asymmetric inertial instability. *J. Atmos. Sci., 46*, 817-831.

Dunkerton, T.J., 1981: On the inertial stability of the equatorial middle atmosphere. *J. Atmos. Sci., 38*, 2354-2364.

Dunkerton, T.J., 1983: A nonsymmetric equatorial inertial instability. *J. Atmos. Sci., 40*, 807-813.

Farrell, B.F., 1982: Pulse asymptotics of the Charney baroclinic instability problem. *J. Atmos. Sci., 39*, 507-517.

Fritts, D.C., L. Yuan, M.H. Hitchman, L. Coy, E. Kudeki, and R.F. Woodman, 1992: Dynamics of the equatorial mesosphere observed using the Jicamarca MST radar during June and August 1987. *J. Atmos. Sci.*, submitted.

Held, I.M., and A.Y. Hou, 1980: Nonlinear axially symmetric circulations in a nearly inviscid atmosphere. *J. Atmos. Sci., 37*, 515-533.

Hitchman, M.H., and C.B. Leovy, 1986: Evolution of the zonal mean state in the equatorial middle atmosphere during October 1978-May 1979. *J. Atmos. Sci., 43*, 3159-3176.

Hitchman, M.H., C.B. Leovy, J.C. Gille, and P.L. Bailey, 1987: Quasi-stationary zonally asymmetric circulations in the equatorial lower mesosphere. *J. Atmos. Sci., 44*, 2219-2236.

Holton, J.R., 1975: *The Dynamic Meteorology of the Stratosphere and Mesosphere.* Amer. Meteor. Soc., 319pp.

Hoskins, B.J., M.E. McIntyre, and A.W. Robertson, 1985: On the use and significance of isentropic potential-vorticity maps. *Quart. J. Roy. Meteor. Soc., 111*, 877-946.

Huerre, P., and P.A. Monkewitz, 1990: Local and global instabilities in spatially developing flows. *Annu. Rev. Fluid Mech., 22*, 473-537.

Hunt, B.G., 1981: The maintenance of the zonal mean state of the upper atmosphere as represented in a three-dimensional general circulation model extending to 100 km. *J. Atmos. Sci., 38*, 2172-2186.

Jones, S.C., and A.J. Thorpe, 1992: The three-dimensional nature of 'symmetric' instability. *Quart. J. Roy. Meteor. Soc., 118*, 227-258.

Killworth, P.D., and M.E. McIntyre, 1985: Do Rossby-wave critical layers absorb, reflect, or over-reflect? *J. Fluid Mech., 161*, 449-492.

Krishnamurti, T.N., P.K. Jayakumar, J. Sheng, N. Surgi, and A. Kumar, 1985: Divergent circulations on the 30 to 50 day time scale. *J. Atmos. Sci., 42*, 364-375.

Krishnamurti, T.N., D.K. Oosterhof, and A.V. Mehta, 1988: Air-sea interaction on the time scale of 30 to 50 days. *J. Atmos. Sci., 45*, 1304-1322.

Liebmann, B., 1987: Observed relationships between large-scale tropical convection and the tropical circulation on subseasonal time scales during the northern hemisphere winter. *J. Atmos. Sci., 44*, 2543-2561.

Matsuno, T., 1966: Quasi-geostrophic motions in the equatorial area. *J. Meteor. Soc. Japan, 44*, 25-43.

O'Sullivan, D.J., and M.H. Hitchman, 1992: Inertial instability and Rossby wave breaking in a numerical model. *J. Atmos. Sci., 49*, 991-1002.

Philander, G., 1989: *El Niño, La Niña, and the Southern Oscillation.* Academic Press, 293 pp.

Pierrehumbert, R.T., 1984: Local and global baroclinic instability of zonally varying flow. *J. Atmos. Sci., 41*, 2141-2162.

Pierrehumbert, R.T., 1986: Spatially amplifying modes of the Charney baroclinic instability problem. *J. Fluid Mech., 170*, 293-317.

Stevens, D.E., 1983: On symmetric stability and instability of zonal mean flows near the equator. *J. Atmos. Sci., 40*, 882-893.

Stevens, D.E., and P. Ciesielski, 1986: Inertial instability of horizontally sheared flow away from the equator. *J. Atmos. Sci., 43*, 2845-2856.

Thorpe, A.J., and R. Rotunno, 1989: Nonlinear aspects of symmetric instability. *J. Atmos. Sci., 46*, 1285-1299.

Publication list for

Dr. Timothy J. Dunkerton

1. Stanford, J.L., and T.J. Dunkerton, 1977: The character of ultra-long stratospheric temperature waves during the 1973 Austral winter. *Beitrage zur Physik dur Atmosphare, 51,* 174-188.

2. Holton, J.R., and T.J. Dunkerton, 1978: On the role of wave transience and dissipation in stratospheric mean flow vacillations. *J. Atmos. Sci., 35,* 740-744.

3. Dunkerton, T.J., 1978: On the mean meridional mass motions of the stratosphere and mesosphere. *J. Atmos. Sci., 35,* 2325-2333.

4. ——, 1979: On the role of the Kelvin wave in the westerly phase of the semiannual zonal wind oscillation. *J. Atmos. Sci., 36,* 32-41.

5. ——, 1980: A Lagrangian mean theory of wave, mean-flow interaction with applications to nonacceleration and its breakdown. *Rev. Geophys. Space Phys., 18,* 387-400.

6. ——, 1981: Wave transience in a compressible atmosphere, Part I: transient internal wave, mean-flow interaction. *J. Atmos. Sci., 38,* 281- 297.

7. ——, 1981: Wave transience in a compressible atmosphere, Part II: transient equatorial waves in the quasi-biennial oscillation. *J. Atmos. Sci., 38,* 298-307.

8. ——, C.-P. F. Hsu, and M.E. McIntyre, 1981: Some Eulerian and Lagrangian diagnostics for a model stratospheric warming. *J. Atmos. Sci., 38,* 819- 843.

9. Dunkerton, T.J., 1981: On the inertial stability of the equatorial middle atmosphere. *J. Atmos. Sci., 38,* 2354-2364.

10. ——, 1982: Curvature diminution in equatorial wave, mean-flow interaction. *J. Atmos. Sci., 39,* 182-186.

11. ____, 1982: Shear zone asymmetry in the observed and simulated quasi-biennial oscillations. *J. Atmos. Sci., 39,* 461-469.

12. ____, 1982: Wave transience in a compressible atmosphere, Part III: the saturation of internal gravity waves in the mesosphere. *J. Atmos. Sci., 39,* 1042-1051.

13. ____, 1982: The double-diffusive modes of symmetric instability on an equatorial beta-plane. *J. Atmos. Sci., 39,* 1653-1657.

14. ____, 1982: Stochastic parameterization of gravity wave stresses. *J. Atmos. Sci., 39,* 1711-1725.

15. ____, 1982: Theory of the mesopause semiannual oscillation. *J. Atmos. Sci., 39,* 2682-2690.

16. ____, 1983: The evolution of latitudinal shear in Rossby-gravity wave, mean-flow interaction. *J. Geophys. Res., 88,* 3836-3842.

17. ____, 1983: A nonsymmetric equatorial inertial instability. *J. Atmos. Sci., 40,* 807-813.

18. ____, 1983: Laterally-propagating Rossby waves in the easterly acceleration phase of the quasi-biennial oscillation. *Atmos.-Ocean, 21,* 55-68.

19. ____, 1983: Modification of stratospheric circulation by trace constituent changes? *J. Geophys. Res., 88,* 10831-10836.

20. ____, 1983: On the conservation of pseudoenergy in Lagrangian time-mean flow. *J. Atmos. Sci., 40,* 2623-2629.

21. ____, and D.C. Fritts, 1984: The transient gravity wave critical layer, Part I: convective adjustment and the mean zonal acceleration. *J. Atmos Sci., 41,* 992-1007.

22. ____, and N. Butchart, 1984: Propagation and selective transmission of internal

gravity waves in a sudden warming. *J. Atmos. Sci., 41,* 1443- 1460.

23. Fritts, D.C., and T.J. Dunkerton, 1985: Fluxes of heat and constituents due to convectively unstable gravity waves. *J. Atmos. Sci., 42,* 549- 556.

24. ____, and ____, 1984: A quasi-linear study of gravity wave saturation and self-acceleration. *J. Atmos. Sci., 41,* 3272-3289.

25. Dunkerton, T.J., 1984: Inertia-gravity waves in the stratosphere. *J. Atmos. Sci., 41,* 3396-3404.

26. ____, and D.P. Delisi, 1985: Climatology of the equatorial lower stratosphere. *J. Atmos. Sci., 42,* 376-396.

27. Dunkerton, T.J., 1985: A two-dimensional model of the quasi-biennial oscillation. *J. Atmos. Sci., 42,* 1151-1160.

28. ____, and D.P. Delisi, 1985: The subtropical mesospheric jet observed by the Nimbus 7 Limb Infrared Monitor of the Stratosphere. *J. Geophys Res., 90,* 10681-10692.

29. ____, and ____, 1986: Evolution of potential vorticity in the winter stratosphere of January-February 1979. *J. Geophys. Res., 91,* 1199-1208.

30. Dunkerton, T.J., 1987: Resonant excitation of hemispheric barotropic instability in the winter mesosphere. *J. Atmos. Sci., 44,* 2239-2251.

31. ____, 1987: Effect of nonlinear instability on gravity wave momentum transport. *J. Atmos. Sci., 44,* 3188-3209.

32. ____, 1988: Body force circulation and the Antarctic ozone minimum. *J. Atmos. Sci., 45,* 427-438.

33. ____, 1989: Theory of internal gravity wave saturation. *Pure and Appl. Geophys., 130,* 373-397.

34. ____, D.P. Delisi, and M.P. Baldwin, 1988: Distribution of major stratospheric warmings in relation to the quasi-biennial oscillation. *Geophys. Res. Lett., 15,* 136-139.

35. Dunkerton, T.J., 1989: Body force circulations in a compressible atmosphere: key concepts. *Pure and Appl. Geophys., 130,* 243-262.

36. Delisi, D.P., and T.J. Dunkerton, 1988: Equatorial semiannual oscillation in zonally averaged temperature observed by the Nimbus 7 SAMS and LIMS. *J. Geophys. Res., 93,* 3899-3904.

37. ____, and ____, 1989: Laboratory observations of gravity wave critical-layer flows. *Pure and Appl. Geophys., 130,* 445-461.

38. ____, and ____, 1988: Seasonal variation of the semiannual oscillation. *J. Atmos. Sci., 45,* 2772-2787.

39. Dunkerton, T.J., 1989: Nonlinear Hadley circulation driven by asymmetric differential heating. *J. Atmos. Sci., 46,* 956-974.

40. Baldwin, M.P., and T.J. Dunkerton, 1989: The stratospheric major warming of early December 1987. *J. Atmos. Sci., 46,* 2863-2884.

41. Dunkerton, T.J., 1989: Eigenfrequencies and horizontal structure of divergent barotropic instability originating in tropical latitudes. *J. Atmos. Sci., 47,* 1288-1301.

42. Baldwin, M.P., and T.J. Dunkerton, 1989: Observations and statistical simulations of a proposed solar cycle/QBO/weather relationship. *Geophys. Res. Lett., 16,* 863-866.

43. Gray, L.J., and T.J. Dunkerton, 1990: The role of the seasonal cycle in the quasi-biennial oscillation of ozone. *J. Atmos. Sci., 47,* 2429-2451.

44. Dunkerton, T.J., 1990: Annual variation of deseasonalized mean flow acceleration in the equatorial lower stratosphere. *J. Meteor. Soc. Japan, 68,* 499-508.

45. ____, 1991: Nonlinear propagation of zonal winds in an atmosphere with Newtonian cooling and equatorial wavedriving. *J. Atmos. Sci., 48,* 236-263.

46. ____, and M.P. Baldwin, 1991: Quasi-biennial modulation of planetary wave fluxes in the Northern hemisphere winter. *J. Atmos. Sci., 48,* 1043-1061.

47. ____, 1991: LIMS observation of traveling planetary waves and potential vorticity advection in the stratosphere and mesosphere. *J. Geophys. Res., 96,* 2813-2834.

48. ____, and D.P. Delisi, 1991: Anomalous temperature and zonal wind in the tropical upper stratosphere, 1982/83. *J. Geophys. Res., 96,* 22,631-22,641.

49. ____, and F.X. Crum, 1991: Scale selection and propagation of wave-CISK with conditional heating. *J. Meteor. Soc. Japan, 69,* 449-458.

50. Baldwin, M.P., and T.J. Dunkerton, 1991: Quasi-biennial oscillation above 10 mb.*Geophys. Res. Lett., 18,* 1205-1208.

51. Dunkerton, T.J., 1991: Intensity variation and coherence of 3-6 day equatorial waves. *Geophys. Res. Lett., 18,* 1469-1472.

52. Crum, F.X., and T.J. Dunkerton, 1992: Analytic and numerical models of wave-CISK with conditional heating. *J. Atmos. Sci.,* 1693-1708.

53. Dunkerton, T.J., and R.E. Robins, 1992: Radiating and nonradiating modes of secondary instability in a gravity wave critical layer. *J. Atmos. Sci.,* 2546-2559.

54. ____, and ____, 1992: Evidence of saturation in a gravity wave critical layer. *J. Atmos. Sci.,* 2560-2563.

55. ____, and M.P. Baldwin, 1992: Modes of interannual variability in the stratosphere. *Geophys. Res. Lett., 19,* 49-52.

56. ____, 1992: Inertial instability of nonparallel flow on an equatorial beta-plane. *J.*

Atmos. Sci, to appear.

57. ——, 1992: Observation of 3-6 day meridional wind oscillations over the tropical Pacific, 1973-1992: vertical structure and interannual variability. *J. Atmos. Sci*, to appear.

58. Crum, F.X., and T.J. Dunkerton, 1993: CISK and evaporation-wind feedback with conditional heating on an equatorial beta-plane. . *J. Meteor. Soc. Japan*, submitted.

59. O'Sullivan, D.J., and T.J. Dunkerton, 1993: Seasonal development of the extratropical QBO in a numerical model of the middle atmosphere: sensitivity to external forcings. *J. Atmos. Sci.*, submitted.